



Ademe



document public

Geological and petrophysical parameters of a deep fractured sandstone formation as applied to geothermal exploitation

EPS-1 borehole, Soultz-sous-Forêts, France

* J.F. Vernoux, * A. Genter, * P. Razin, ** C. Vinchon

december 1995
Rapport du BRGM R 38622

* BRGM, Orléans
** BRGM, Nord-Pas de Calais

BRGM
DIRECTION DE LA RECHERCHE
Département Hydrologie, Géochimie et Transferts
BP 6009 - 45060 ORLEANS CEDEX 2 - France - Tél.: (33) 38 64 34 34

Mots clés : Geothermal exploitation, Argillaceous sandstone, Sedimentological processes, Diagenesis, Fracture network, Reservoir, Porosity, Permeability, Soultz-sous-Forêts borehole, Rhinegraben, France

En bibliographie, ce rapport sera cité de la façon suivante :

VERNOUX J.F., GENTER A., RAZIN P., VINCHON C. (1995) - Geological and petrophysical parameters of a deep fractured sandstone formation as applied to geothermal exploitation, EPS-1 borehole, Soultz-sous-Forêts, France, Rapport BRGM R 38622, 70 p., 24 fig., 5 tabl., 3 append.

© BRGM, 1995, ce document ne peut être reproduit en totalité ou en partie sans l'autorisation expresse du BRGM.

ABSTRACT

In the framework of a European research project dealing with the improvement of the injectivity index of argillaceous sandstone, a basic study of a potential geothermal clastic aquifer was carried out from an exhaustive analysis of deep well data.

A core from the base of Mesozoic cover rocks intersected in borehole EPS-1 (Soultz-sous-Forêts, Rhine Graben, France) provided a continuous section of the Buntsandstein sandstones (1009-1417m), considered as a potential geothermal reservoir. More than 400 m length of continuous core sections were analyzed in details in terms of sedimentological features, diagenetic evolution, pre-existing fracturation and petrophysical properties in order to define the best potential reservoirs within this deep clastic formation.

This multidisciplinary study shows that the occurrences of present-day potential permeable zones, namely reservoir, are controlled (i) by the early sedimentological processes of this clastic unit (regression and transgression cycles), (ii) by the diagenetic evolution which partly decreased the porosity of the initial reservoirs and (iii) by the intense fracturing which enabled hydrothermal fluid to circulate within the fracture network and to cement partly the matrix porosity and the fractures by mineral filling.

The best potential reservoirs were the sandstone bars built by the large fluvial system of the Vosgian sandstone during a period of strong vertical aggradation, i.e. during transgressive phases. It represented a thickness of more than 200 m.

Petrographic and diagenetic studies showed that the Triassic sandstones underwent many diagenetic events (early diagenesis, pedogenesis, burial diagenesis, diagenesis related to fluid circulation in fractures), characterized by mineral precipitation (sparitic nodules, quartz overgrowth, clay minerals, barite) and dissolution (feldspar alteration).

Detailed structural analysis of continuous core samples indicated that the dominating nearly-vertical fracture network is oriented N-S in accordance with the local Soultz horst structure. Mechanically, the Triassic sandstones represent a competent lithological formation and the natural fractures encountered in the EPS-1 core sections showed a clustering organization (fault zone) combined with significant mineral infilling (mainly barite). The average fracture density is 0,85 fr/m with a maximum of 5 fr/m located within a major faulted zone at 1200 m depth.

From an exhaustive petrophysical database, the relationship between different kinds of porosity (sonic, mercury, gamma-density derived) and gas permeability was investigated. In EPS-1 sandstones, the variation of permeability can be very important even on a few cm-scale. If there is no relation between permeability and porosity, a good correlation is obtained between permeability and macro-porosity derived from mercury porosimetry. The large heterogeneity of permeability is strongly controlled by the heterogeneous pore-space geometry. Initial sediment composition and diagenetic evolution are the two main factors responsible for the current geometry of porous network.

A comparison between porosity profiles, fracture density profile and permeability profile with depth showed that the best clastic reservoir is located within a depth interval depleted in fractures. From this integrated study based on the evaluation of geological and petrophysical properties of a thick-argillaceous sandstone formation (Triassic sandstones), sampled in a deep well, a potential geothermal reservoir was expected between 1115 and 1160 m depth. This reservoir has an attractive temperature (120°) but medium permeability (about 100 mD) and contains minerals in porous matrix, like clays, which can have a negative effect on a future exploitation.

CONTENTS

INTRODUCTION.....	10
1. GEOLOGICAL SETTING.....	12
2. EQUIPMENTS AND METHODS.....	16
2.1. Structural analysis of core.....	16
2.2. Preparation of plugs.....	16
2.3. Petrographic study.....	16
2.4. Petrophysical measurements.....	17
2.4.1. Porosity.....	17
2.4.2. Permeability.....	18
3. DEPOSITIONAL FEATURES AND LITHOFACIES.....	19
3.1. Annweiler Sandstone.....	19
3.2. Vosgian Sandstone.....	19
3.3. Intermediate Beds.....	20
3.4. Voltzia Sandstone.....	21
3.5. Initial reservoir quality.....	21
4. FRACTURATION OF DEEP CLASTIC RESERVOIR.....	23
4.1. Basin stress history.....	23
4.2. Typology of structures.....	23
4.2.1. Early clastic dikes.....	23
4.2.2. Brittle structures.....	23
4.3. Fracture properties versus depth.....	23
4.3.1. Structure density versus depth.....	24
4.3.2. Profile of cumulative fracture width.....	25
4.3.3. Profile of fracture filling.....	25
4.4. Fracture characterization.....	26
4.4.1. Geometry of the natural fracture system.....	26
4.4.2. Fracture orientation with depth.....	27
4.4.3. Fracture width.....	28

4.4.4. Fracture free aperture	32
4.5. Influence of tectonic features on the joint network for evaluation of clastic geothermal reservoir	32
5. PETROGRAPHY AND DIAGENESIS	36
5.1. Initial sediment composition.....	36
5.2. Diagenesis.....	36
5.2.1. Pedogenetic diagenesis	36
5.2.2. Early burial diagenesis.....	37
5.2.3. Impact of late burial and tectonism on diagenesis	37
6. PETROPHYSICAL PARAMETERS.....	40
6.1. Porosity and pore space	40
6.2. Permeability	44
7. RESERVOIR QUALITY EVOLUTION	48
7.1. Lithological sub-units of Lower Triassic sandstones	48
7.2. Reservoir quality evolution through diagenesis	48
7.3. Current reservoir quality.....	50
CONCLUSION	52
REFERENCES	54
APPENDICES	58

LIST OF FIGURES

- Figure 1 Structural map of the Rhine graben and wells location.
EPS-1 and GPK-1 wells (Soultz area)
GCR- 1 well (Strasbourg area)
- Figure 2 Lithological section of the deep Triassic (Muschelkalk, Buntsandstein) and Permian formations in the EPS-1 borehole. The Gamma Ray (GR) curve points out the main sub-units of these deep triassic levels.
- Figure 3 Geological cross section of the Soultz site based on seismic reflexion profiles within the sedimentary cover intersecting GPK-1 borehole. EPS-1 borehole is located at 500 m SE of GPK-1 [after *Cautru in Menjoz et al., 1988; modified Genter and Traineau, 1993*].
- Figure 4 Open fracture visible both on core and on oriented BHTV borehole imagery at 1205 m in EPS-1well.
- Figure 5 Undercoring and sampling for thin sections, mercury porosimetry and permeability measurements
- Figure 6 Profiles of the overall natural fractures frequency per meter and of the frequency of different types of structure (tension fissure, fault, dry fissure, normal fault, clastic dike) observed on the core section of the EPS-1 well and profile of the cumulative fracture width expressed in mm per meter.
- Figure 7 Profiles of the various hydrothermal or organic fracture filling versus depth observed on the core section of the EPS-1 well.
- Figure 8 Rose diagram of strike azimuth of overall fracture population in EPS-1 well (N=322 data).
- Figure 9 Frequency histograms of fracture dips between 0 and 90 for all the natural fracture population (N= 322 data) observed on the EPS-1 core sections.
(A) Uncorrected dip values.
(B) Corrected dip values according to the method of Terzaghi (1965).
- Figure 10 Lower hemisphere schmidt projection of pole of natural fractures and Kamb contour of pole densities in Buntsandstein of the EPS-1 well (1008 - 1418 m) from core analysis.
A - overall population
B - density plot of overall population (N= 322 data)
C - Clastic dike (N= 37 data)
- Figure 11 Profiles of macroscopic natural fractures observed in the core section of the EPS-1 well.
A - Fracture dip direction
B - Fracture dip
- Figure 12 Frequency histograms of fracture sealed width (A), of fracture free aperture (B) and profile of fracture free aperture versus depth (C) measured on the core sections of the EPS-1 well.

- Figure 13 Main diagenetic phases observed in the Buntsandstein sandstones of the EPS-1 well
- Figure 14 Plot of sonic-log-derived porosity vs. gamma-density-derived porosity
- Figure 15 Plot of mercury-porosimetry-derived porosity vs. gamma-density-derived porosity
- Figure 16 Capillary pressure curves for 6 samples of EPS-1 sandstones
- Figure 17 Withdrawal efficiency vs. porosity for the four main Buntsandstein levels
- Figure 18 Plot of pore-throat-size distribution (PTD) vs. porosity for the four main Buntsandstein level.
- Figure 19 Semi-log plot of permeability vs. porosity.
- Figure 20 Semi-log plot of permeability vs. macro-porosity.
- Figure 21 Plot of macro-porosity vs. $(S_{Hg} / P_c)_{max}$.
- Figure 22 Semi-log plot of shaliness index vs. permeability for the four main Buntsandstein units.
- Figure 23 Synthetic composite log of Lower Triassic sandstones (Buntsandstein) from core analysis in the EPS-1 well (Alsace, France). Formation names are given according to M nillet et al. (1989). Gamma Ray curve gives the natural radioactivity, gamma porosity is deduced from continuous gamma-density measurements performed on core sections, sonic porosity is deduced from well logging data, mercury porosity is measured on selected samples, joint density is recorded from core analysis and gas permeability is performed on selected samples.
- Figure 24 Sedimentological log of EPS-1 borehole. Location of initial and current reservoirs.

LIST OF TABLES

- Table 1** **Successive paleostress fields and associated brittle structures affecting the Upper Rhine graben and its surrounding area (Bergerat, 1985 ; Schneider, 1984 ; Villemin, 1986 ; Villemin and Bergerat, 1987)**
- Table 2** **Amount of different types of macroscopic structures recorded on the Buntsandstein core section of the EPS-1 well and successfully oriented.**
- Table 3** **Structural data orientation within Buntsandstein formation**
- Table 4** **Parameters derived from mercury porosimetry**
- Table 5** **Influence of macro-porosity on permeability**

LIST OF APPENDICES

- 1. Photographic plates**
Plate 1: Photo 1 to 6
Plate 2: Photo 1 to 7
Plate 3: Photo 1 to 5
- 2. Petrophysical data for the 67 cored samples of the EPS-1 borehole**
- 3. Semi quantitative analysis of mineral phases**

INTRODUCTION

The NW part of the Rhine graben in France is characterized by a geothermal anomaly which can reach more than 8°C/100 m in the Soultz area (Schellschmidt and Schultz, 1991; Flores and Royer, 1992; Vernoux and Lambert, 1993) and by a complex extensional framework (Fig. 1).

The attempts to exploit the geothermal resources in Alsace gave limited results and only carbonate reservoirs are exploited for balneology. But the most interesting formation in term of temperature and thickness is the Buntsandstein which is mainly composed of sandstones. In 1980, GCR1 drilling at Cronenbourg (Fig. 1) reached 3220 m with a 150°C temperature but only a 30 m³/h flow rate (Housse, 1984).

This brief historical account shows that the geothermal gradient is not the only parameter which conditions the profitability of geothermal exploitation. Sandstone reservoir quality is determined by permeability which depends on geological parameters, (i) depositional features for the geometry of initial porous and isolating bodies, (ii) fracturation associated to tectonic events and (iii) diagenetic alteration induced by sedimentary or tectonic events.

It is now well recognised that the description of facies is more adequate to describe the properties of the underground, especially the connectivity between beds, than classical stratigraphy (Marsily, 1993). The porosity and the pore throat system which control matrix permeability can be strongly affected by diagenesis (Moraes, 1991). A geothermal exploitation requires, in most cases, to reinject the heat-depleted fluid in the reservoir. The permeability of the reservoir, near the wellbore, can dramatically decrease, due to plugging by mineral particles, especially clays (Ochi *et al.*, 1993; Vinchon *et al.*, 1993). The type and mode of occurrence of clay minerals depend on the depositional features and diagenetic alteration processes (Pittman and Thomas, 1979). Finally the connectivity, which conditions fluid circulation, is also strongly influenced by the fracturation, well developed in the Rhine graben. The fractures system can increase the permeability when the fractures are open but, according to its geometry, it can also create short cuts between the production and injection wells and decrease the lifetime of the doublet. On the opposite, when the fractures are filled with minerals, they create impervious barriers and limit the extension of the reservoir.

The drilling of several deep wells in the framework of the Hot Dry Rock project at Soultz (Fig. 1) gave the opportunity to dispose of a 400 m continuous cored section of Buntsandstein sandstones and well logging data. The purpose of this study is to investigate the interest of Buntsandstein sandstones for geothermal exploitation in France and to show how the combination of petrophysical, lithological, diagenetic and fracturation parameters can help to define reservoir and non-reservoir facies in a complex extensional framework.

This work was carried out in the framework of a BRGM research program about the geothermal exploitation of sandstone reservoirs (project EG50, then S06). It was supported by European Community (DG XII, Joule II programme, Contract CT92-0183) and ADEME (Agence de l'Environnement et de la Maitrise de l'Energie). This report contains all relevant results obtained from the study of EPS-1 triassic sandstones, relative to depositional features and lithofacies, fracturation, diagenesis and petrophysics.

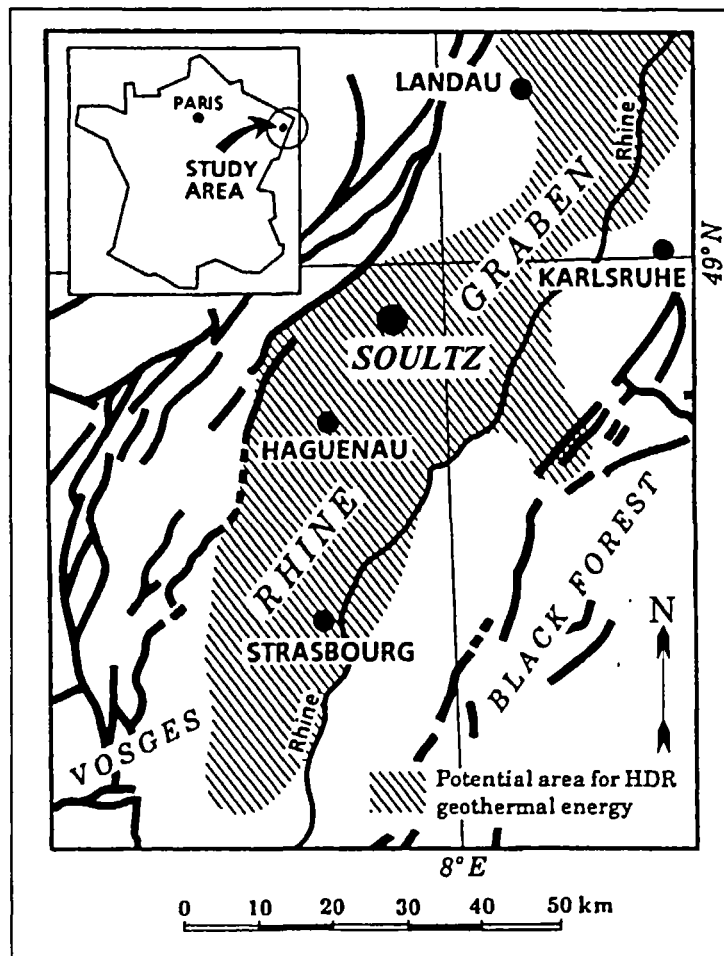


Fig. 1 - Structural map of the Rhine graben and wells location
EPS-1 and GPK-1 wells (Sultz area)
GCR- 1 well (Strasbourg area)

1. GEOLOGICAL SETTING

The site is located near the western part of the Upper Rhine graben (Fig. 1). This structure belongs to the western European cenozoic rifts systems. It extends NNE-SSW over a distance of 300 km and has a width of 30-40 km.

The Rhine Graben has been tectonically active since the late Eocene (Ziegler, 1992) with a marked subsidence rate. In the Soultz basin, 10-meters-thick of Permian silico-clastic sediments (conglomerate, sandstone) observed in EPS-1 lying directly on the Hercynian granite pointed out an erosion period of the variscan chain. Mesozoic formations are only represented by Triassic and a part of Jurassic levels.

In EPS-1 well, the stratigraphic limits of Buntsandstein sandstones (Fig. 2) were deduced from nuclear well-logging measurements (Gamma Ray curve) and from comparison between core section and outcrops (Ménillet et al., 1989). EPS-1 was initially drilled for oil and gas exploration. The triassic sedimentary cover was drilled non-coring from 830 to 930 m and then cored continuously to the contact with the granite at 1417 m. This continuous coring provides the first opportunity to characterise naturally fractured deep triassic reservoirs within the Rhine graben.

Due to emersion of this area during Cretaceous-Paleocene period, the Eocene formations occurred directly on the Jurassic levels. After an initial North-South compressive stage (Villemin, 1986; Bergerat, 1987; Villemin and Bergerat, 1987), high subsidence rate related to a general extensional regime takes place during late Eocene and Oligocene times. Evolution of the Rhine Graben has been governed by the extension due to the interaction of the Eurasian and African plates (Ziegler, 1992).

GPK-1 and EPS-1 boreholes are located inside the graben, 5 km from its western border represented by the master Rhenan Fault oriented N30E-N40E (Ménillet et al., 1989). Schematic geological cross section of the Rhine graben (Maget et al., 1979; Schnaebeler, 1948) gives the main relations between the geometry of Buntsandstein surface and the normal fault network (Fig. 3). A 3-D geometric modelling of fault and layer systems in the Soultz area using GOCAD software was performed in order to obtain a better understanding of the structural properties of this site (Chiles et al., 1993; Renard and Courrioux, 1994).

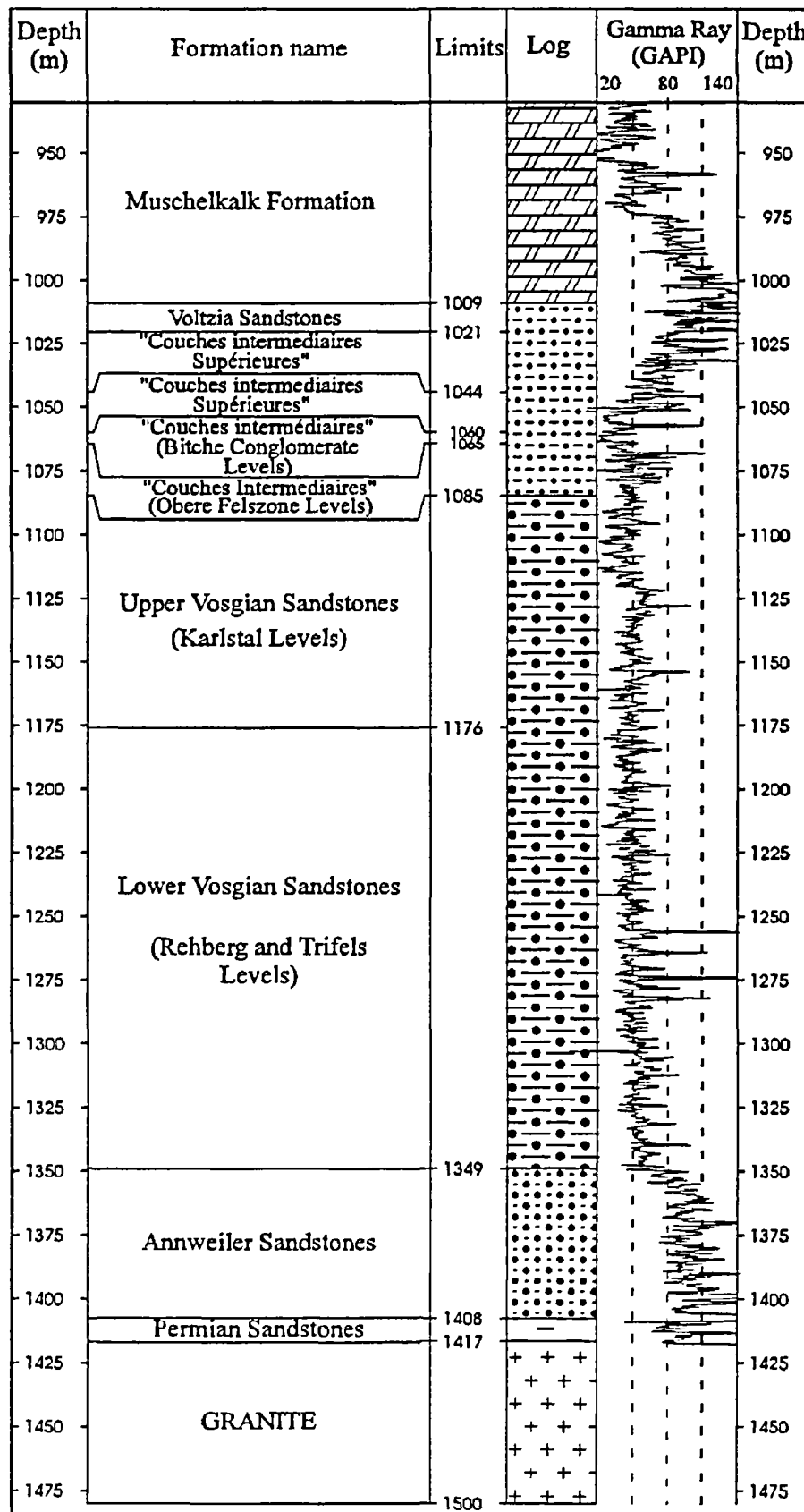


Fig. 2 - Lithological section of the deep Triassic (Muschelkalk, Buntsandstein) and Permian formations in the EPS-1 borehole. The Gamma Ray (GR) curve points out the main sub-units of these deep triassic levels.

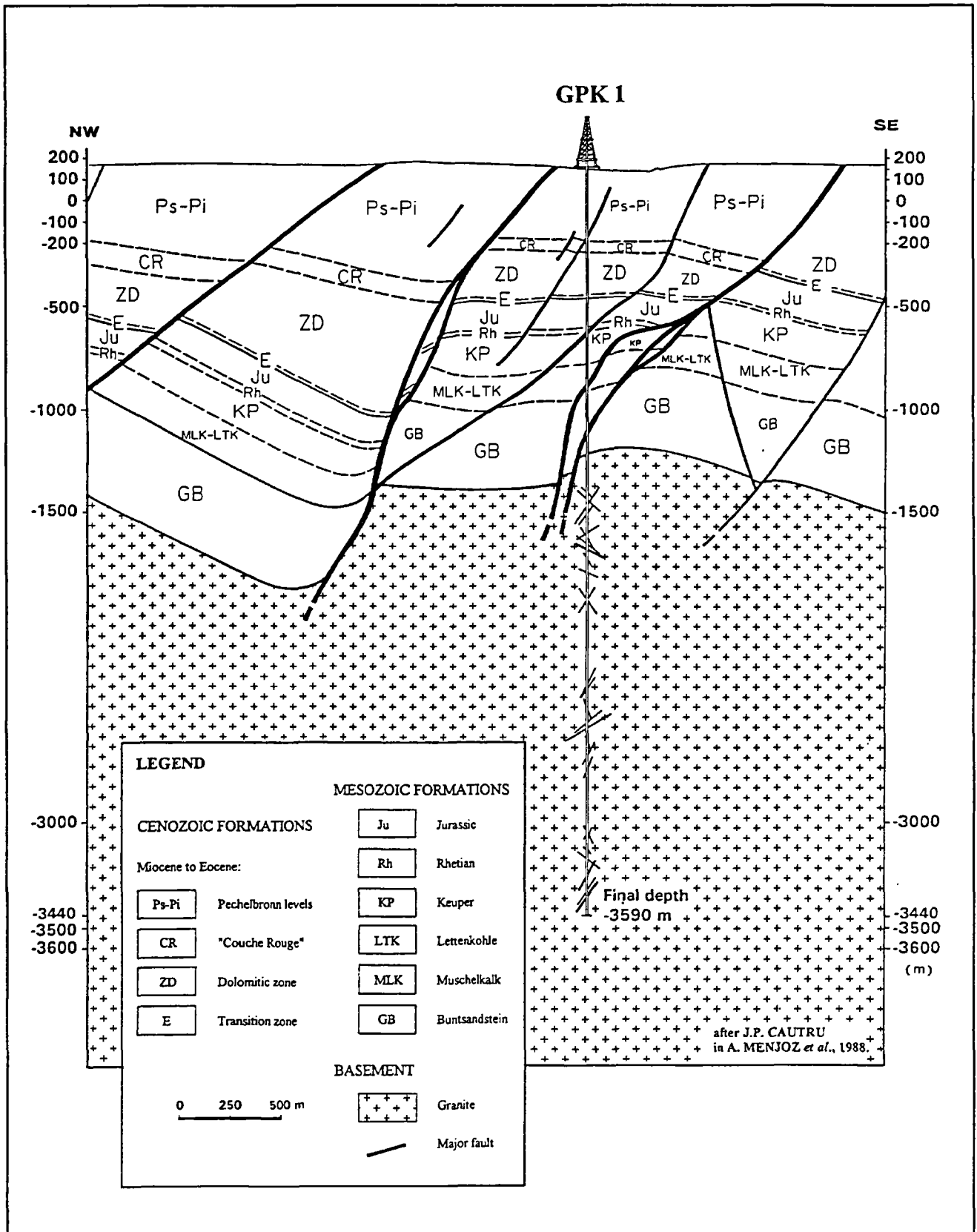


Fig. 3 - Geological cross section of the Soultz site based on seismic reflexion profiles within the sedimentary cover intersecting GPK-1 borehole. EPS-1 borehole is located at 500 m SE of GPK-1 [after Cautru in Menjoz *et al.*, 1988; modified Genter and Traineau, 1993].

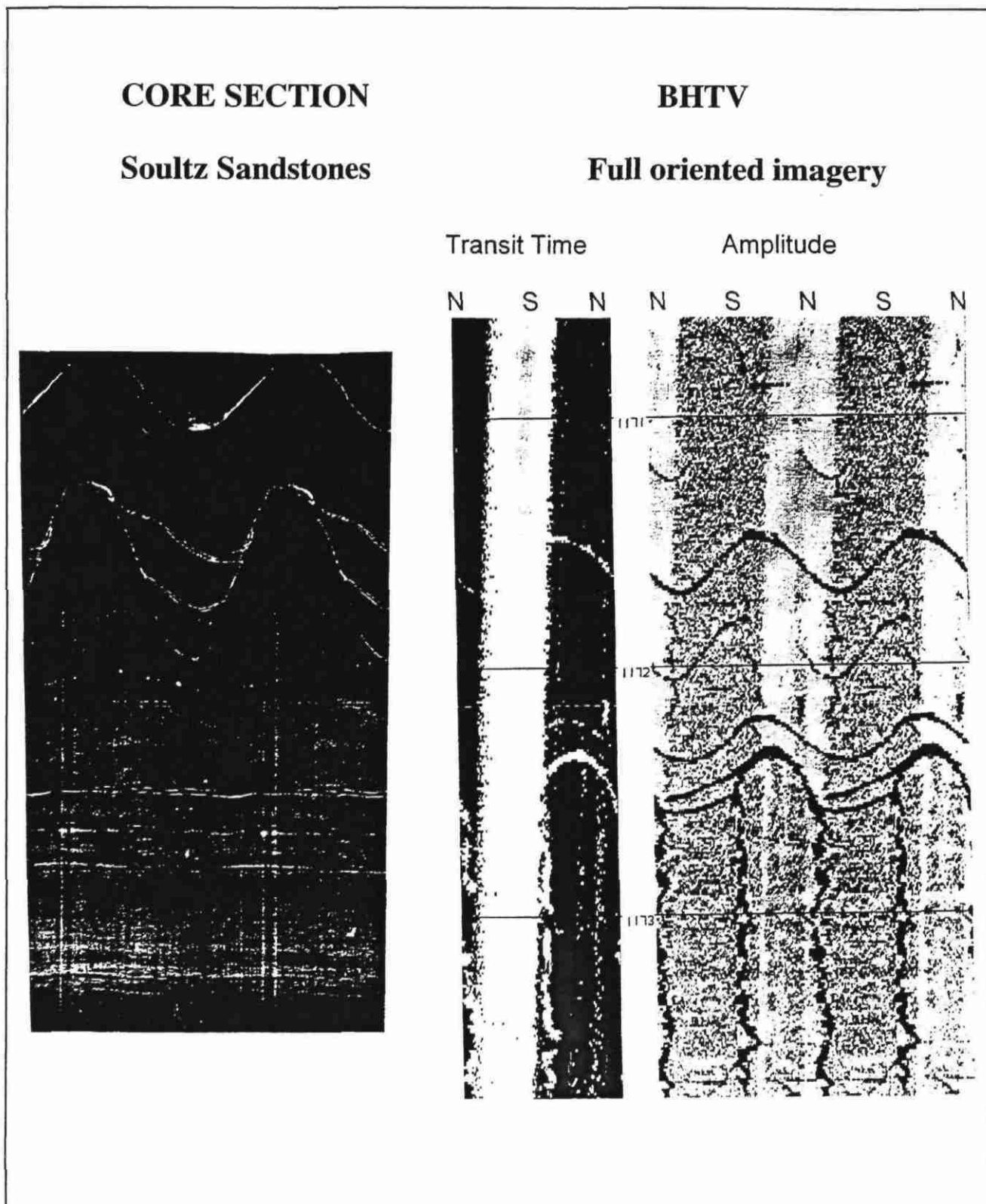


Fig. 4 - Open cluster of fractures visible both on core and on oriented BHTV borehole imagery at 1173 m in EPS-1 well.

2. EQUIPMENTS AND METHODS

2.1. STRUCTURAL ANALYSIS OF CORE

The core pieces in which structural features were present were photocopied using an unrolled photocopy machine which produces flatcore copies at 1/1 scale. The fracture traces were then analysed and recorded by the digitiser using the BRGM GDM (Geological Data Management) software. For each feature, the following parameters were entered into the structural data base:

- type of discontinuity and associated striation marks,
- orientation in the horizontal plane according to the arbitrary reference line,
- dip according to the arbitrary reference line,
- depth of the planar discontinuity along the borehole,
- nature of filling, in chronological order when possible,
- true thickness of hydrothermal fillings,
- free aperture.

The natural fractures were generally sealed during one or more episodes of hydrothermal deposition, which were identified in hand-specimen. The minerals include quartz, barite, galena, pyrite, calcite and hematite. Organic compounds were observed associated to hydrothermal filling. During the survey of EPS-1 borehole, the core sections were not directly oriented at the drill site. An ad hoc procedure was developed for the evaluation of the structural features occurring in the core (Genter and Traineau, 1992). All the core pieces were put together and marked with a common reference line, this line being used later for the reorientation of the cores through Borehole Televiewer imagery (Tenzer et al., 1992). The basic method consists in identifying a single feature visible both on the core and on the acoustic oriented imagery. Open fracture is the most characteristic structure detectable on both borehole imagery and core (Fig. 4). 348 structures were recorded on the cores and 322 of them were reoriented with a degree of accuracy estimated to 10° approximately (Table 2).

2.2. PREPARATION OF PLUGS

A set of 67 samples was selected from the 400 m Buntsandstein sandstones cores in the non fractured zones. The plugs (4 cm diameter and 4.5 cm length) were obtained by air drilling in the flow direction. Splinters and thin sections were also prepared for mercury porosimetry and petrographic analysis (Fig. 5).

2.3. PETROGRAPHIC STUDY

The diagenetic sequences and their relative chronology were determined through classical petrographic analysis of sediment and fracture fillings. Components amounts given herein are semi-quantitative estimations based on visual evaluation with the Chillingar chart. In this report, the aim is to describe the diagenetic mineralisations in terms of reservoir evolution.

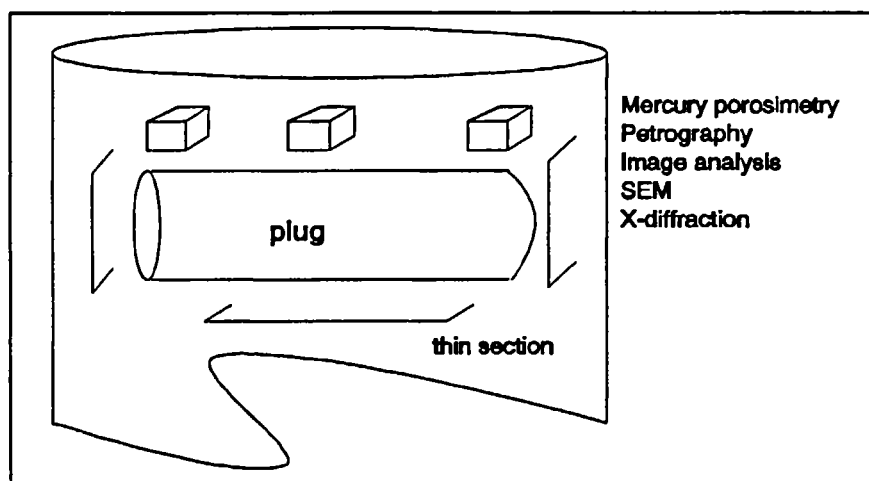


Fig. 5 - Undercoring and sampling for thin sections, mercury porosimetry and permeability measurements

2.4. PETROPHYSICAL MEASUREMENTS

2.4.1. Porosity

Porosity measurements were realised with three different methods: sonic log, gamma-density on cores, mercury porosimetry.

Sonic porosity. The sonic porosity was calculated from an acoustic log realised with a Variable Acoustic Low frequency system:

$$\Phi = \frac{t_l - t_m}{t_f - t_m}$$

where t_l is the measured transit time ($\mu\text{s}/\text{foot}$), t_m is the transit time in the matrix and t_f is the transit time in the fluid. We took values of $86 \mu\text{s}/\text{foot}$ for t_m and $350 \mu\text{s}/\text{foot}$ for t_f (Schlumberger, 1987).

Gamma-density. An equipment developed by BRGM (DIACORE; Dumas, 1990) enables to measure the adsorption of gamma-rays by a material and to deduce its wet density. The porosity of the material is derived from gamma-density by the following relation:

$$\Phi = \frac{\rho_s - \rho_r}{\rho_s(1 - S_w)}$$

where ρ_s is the density of the material, ρ_r is the measured gamma density, and S_w the water saturation.

We took a value of 2.65 for ρ_s which corresponds to the density of siliceous rocks and a zero value for S_w , as the measurements were done several months after well coring. Gamma-density measurements were realised on the whole cored section with a 5 mm interval (Dumas and Delpaume, 1991).

Mercury porosimetry. The mercury porosity measurements were done with a 2000 CARLO ERBA porosimeter under a 0.1 to 2000 bars pressure. The sample volume is about 1 cm^3 . The volume of mercury penetrating the sample is a function of pressure and characteristics of the porous medium. With the assumption of cylindrical pores, the pressure can be converted into pore radius according to the Washburn equation.

$$P_c = -2\gamma \cos\theta / r$$

where P_c is the mercury capillary pressure (bar), γ is the mercury interfacial tension (mN/m), θ is the contact angle and r is the radius of the pore entries (μm)

2.4.2. Permeability

Gas permeability measurements were made with nitrogen at different flow rates without back pressure. A sleeve confining pressure was applied with nitrogen (Vernoux et al., 1993).

The gas flow rate is recorded with a mass flow meter which gives a percentage of the maximum flow rate. It was calibrated for a 1 m³/h nitrogen maximum flow rate. Gas flow in porous medium is more complex than liquid flow and is affected by gas slippage effect (Mc Phee and Arthur, 1991) and non-Darcy effect (Noman and Kalam, 1991). Experimental conditions with high flow rates and mean pressures minimise gas slippage effects and enable to calculate the permeability and the inertial coefficient β by plotting the flow data according to an integrated form of the Forchheimer equation (Noman and Kalam, 1991). β also provides a very sensitive indication of the permeability heterogeneity, on a core-plug level (Jones, 1987).

3. DEPOSITIONAL FEATURES AND LITHOFACIES

A core from the base of the Mesozoic cover rocks intersected in Borehole EPS-1 provides a continuous section of the Buntsandstein sandstone, considered as a potential geothermal reservoir. Sedimentological analysis (lithology, facies sequences, discontinuities, depositional environment, etc.) of this silicoclastic succession has enabled a qualitative evaluation of the initial reservoir properties of the stratigraphic units before the diagenetic and tectonic changes which have given the present reservoir qualities.

The Scythian to lower Anisian Buntsandstein sandstone succession in Borehole EPS-1 was intersected over approximately 400 m (1009 to 1417 m). At 1417 m it lies unconformably on the granitic basement and at 1009 m it is stratigraphically overlain by the transgressive Muschelkalk lagoonal-marine succession (silty argillite, dolomite, evaporites). It is possible, based on outcrop data (Menillet *et al.*, 1989), that a basal Permian unit is present between 1417 and 1407 m, but this has not been formally identified.

From the paleogeographic standpoint the Buntsandstein, which forms the base of the German Triassic (Alberti, 1834), was deposited in a continental cratonic basin with a depocentre in Northern Germany (Ziegler, 1982). The south-western edge of this German Basin formed an elongate NE-SW arm underlying the Vosges-Alsace region under study and was supplied by fluvial sediments from the Southwest. The resultant deposits are continental and predominantly arenaceous, and regionally comprise four major formations (Menillet *et al.*, 1989) all of which were intersected by Borehole EPS-1.

3.1. ANNWEILER SANDSTONE

The Annweiler Sandstone (1417-1349 m; lower Buntsandstein, and basal Permian unit (?)) comprises a succession of upward-fining sequences with erosive bases marked by soft argillaceous pebbles. The sequences, from a decimetre to several metres thick, begin with medium- to fine-grained, cross-bedded, commonly bioturbated sandstone and end with very bioturbated silty-shale interbeds; the tops are commonly marked by a pedogenic dolomitic component. These facies sequences characterise a relatively distal braided fluvial network in which sandy channel deposits alternate with finer grained flood-plain and lacustrine deposits. Globally, the trend of the sedimentological parameters (sand/shale ratio, bioturbation, sedimentary structures, etc.) in these genetic sequences of the Annweiler Sandstone reflect an unsymmetrical transgression-regression cycle for which the maximum flooding period is marked at about 1398 m in the borehole. This cycle can be correlated with Sequence 1 (lower Buntsandstein) of the sequence stratigraphic framework proposed by Aigner and Bachmann (1992).

Owing to the presence of numerous shale intervals and the thinness of the sandy beds, the initial reservoir quality of this basal unit of the Buntsandstein would have been relatively mediocre.

3.2. VOSGIAN SANDSTONE

The Vosgian sandstone (1349-1079 m; middle Buntsandstein) shows an erosive contact with the underlying Annweiler Sandstone, marking a regional discontinuity known as the Lauter unconformity ("discordance de la Lauter"; Dachroth, 1985). In Borehole EPS-1, this formation can be subdivided into two generally upward-fining units.

The lower unit (GV1; 1349-1152.5 m) incorporates the Rehberg and Trifels beds ("couches de Rehberg et Trifels") and the lower part of the Karlstal beds ("couches de Karlstal"; Menillet *et al.*, 1989). It consists mainly of positive, medium-grained, planar- to festoon-cross-bedded sandstone sequences, from one to several metres thick. The bases of the sequences appear to have only slightly channelled the underlying beds and are in places marked by a lag of coarse-grained sandstone with soft pebbles. The tops are generally finer grained,

although argillaceous intervals are rare, and even absent in the lower part of the unit (1349-1274 m). The uppermost part of the upward fining GV1 unit (1175-1152.5 m) comprises weakly cross-bedded, horizontally-bedded or current-rippled sequences of fine-grained sandstone, in places slightly argillaceous.

The homogeneous and relatively thick facies sequences reflect a strong vertical aggradation of a vast braided or slightly sinuous fluvial system in which flood deposits are practically absent. This strong aggradation indicates a generally rising base level (transgression) that followed the regression recorded at the top of the Annweiler sandstone; the facies at the top of unit GV1 indicate decreased fluvial dynamics corresponding with the maximum flooding equivalent. That this transgression occurred in several phases is shown by the stacking pattern of the genetic sequences, which describe eight predominantly upward-fining sequence sets. The best initial reservoirs would have been in the lower and middle parts of the first six sequence sets where strong vertical aggradation combined with a strong hydrodynamic regime favoured the deposition of thick sandstone bodies with little clay.

The upper unit of the Vosgian sandstone (GV2; 1152.5-1079 m) begins with a fairly homogeneous 25-m-thick interval comprising poorly delimited metre-thick sequences of cross- or horizontally-bedded, medium- to coarse-grained sandstone. It shows an erosive contact with the top of the underlying GV1 unit, marking the regional discontinuity known as the Sarre unconformity ("discordance de la Sarre"; Dachroth, 1985) at the base of a coarse-grained interval (Karlstalfelzone) in the median zone of the Karlstal beds (Menillet *et al.*, 1989). The top of this interval is upward fining and grades into fine- to medium-grained sandstone, in places slightly argillaceous, with a horizontal or slightly inclined and locally bioturbated bedding; an evolution that reflects the transgressive character of the base of the GV2 unit. The upper part of this unit indicates a regressive trend marked by the development of fluvial sandstone sequences with erosive bases and planar or festoon cross-bedding.

Unit GV2 thus corresponds to a transgressive-regressive cycle (Sequence 3 of Aigner and Bachmann, 1992) for which the maximum flooding equivalent is marked at about 1110 m in the borehole. As in the underlying GV1 unit, the best initial reservoirs would have been the thick and only slightly argillaceous sandstone sequences formed under high fluvial aggradation during the transgressive part of the cycle.

The top of the Vosgian sandstone is represented by several erosion surfaces indicating maximum regression. In the southern part of the study region, the event is marked by a conglomeratic formation (Main Conglomerate ["le Conglomérat Principal"]) overlain by a weathered horizon (Purple Boundary Zone [la Zone Limite Violette]), neither of which are represented in borehole EPS-1. In the German Basin it is reflected by a very extensive erosion surface known as H Unconformity ("Discordance H"; Richter-Bernburg, 1974). This phase of erosion could in part be responsible for the absence of the most regressive levels in the study region.

3.3. INTERMEDIATE BEDS

The Intermediate Beds formation (upper Buntsandstein; 1079-1019 m) in borehole EPS-1 directly overlies the Vosges Sandstone and can be subdivided into three units. The lower unit (1079-1064 m), known regionally as the "Obere Felszone" (Leppla, 1988), comprises metre-thick fluvial sandstone sequences with erosive bases marked by micro conglomerate lags and clay pebbles. The sequences consist predominantly of festoon-cross- or composite-bedded, medium- to coarse-grained sandstone overlain by thin bioturbated argillaceous beds, and their stacking describes a minor transgression-regression cycle. The overlying, mainly conglomeratic median unit (1064-1044.5 m), corresponding to the Bitche Conglomerate ("Conglomérat de Bitche"; Menillet *et al.*, 1989) in outcrop, consists of two upward-fining sequences that begin with cross-bedded conglomerate (micro conglomerate in the lower sequence) and end with thin black bioturbated argillaceous beds in places (upper sequence) enclosing pedogenic dolomite nodules. The upper unit (1044.5-1019 m) begins with a thin layer of conglomerate and continues with a succession of thin upward-fining, planar cross-bedded, fine-medium-grained sandstone sequences, the bases of which are commonly marked by a lag of coarse-grained sandstone with argillaceous pebbles and fragments of reworked crust or dolomitic nodules. Horizontally-bedded, variably dolomitic argillaceous intervals with numerous pedogenic dolomite nodules mark the tops of the more distal

facies sequences. Three minor transgression-regression cycles (sequence sets) with an overall transgressive tendency are recognised in this upper unit.

Globally, the Intermediate Beds reflect a braided fluvial system characterised by thinner and more differentiated sequences than the thick homogenous sequences of the Vosgian sandstone; the system was probably more complex and more restricted. This change in fluvial pattern is interpreted as due to a tectonic reorganisation of the basin; the tectonic event being indicated by the regional H unconformity separating the two formations and recognised throughout the German Basin (Aigner and Bachmann, 1992).

After a new regressive pulse indicated by the progradation of the Bitche Conglomerate over the Obere Felszone in the lower part of the formation, the Intermediate Beds reflect a general rise of the base level (transgression) and the development of flood-plain facies with traces of pedogenesis at the top of the succession.

Due to facies heterogeneity, numerous sedimentary discontinuities, thinness of the sequences and early dolomitization, the initial reservoir quality of the Intermediate Beds would have been poorer than that of the Vosgian sandstone.

3.4. VOLTZIA SANDSTONE

The Voltzia sandstone (upper Buntsandstein; 1019-1009 m), which regionally terminates the Buntsandstein succession, has a tectonic contact with the underlying Intermediate Beds. This formation, 15-20 m thick in outcrop but only 10 m thick in the borehole, consists of beds, several decimetres thick, of planar cross- and horizontally-bedded fine-grained micaceous sandstone separated by thin argillaceous Beds in places containing abundant vegetal debris. The top of the formation becomes more argillaceous and shows bioturbated heterolithic facies with current ripples and lenticular stratification. This facies marks a transition to the lagoonal argillaceous deposits of the Muschelkalk.

The Voltzia sandstone is interpreted here as fluvial deposits in a distal alluvial plain environment. Although tectonic truncation does not allow the base of the succession to be seen in the borehole, regional data show a sedimentary discontinuity related to a drop in the base level at the boundary between the two formations of the upper Buntsandstein (Aigner and Bachmann, 1992; Friedenberg, 1994). The Voltzia sandstone then shows a transgressive evolution that led to retrogradation of the lagoonal deposits on the alluvial plain deposits.

Due to the thinness of the sequences and the presence of numerous shale interbeds, the Voltzia Sandstone would not have been a good initial reservoir.

3.5. INITIAL RESERVOIR QUALITY

In conclusion, the Buntsandstein sandstone succession intersected by Borehole EPS-1 comprises five main depositional sequences that fall within the sequential stratigraphic framework defined for the German Basin (Aigner and Bachmann, 1992). After an initial transgressive episode, the basal sequence, corresponding to the Annweiler Sandstone, mainly marks the regressive tendency that characterises the Permian-Triassic transition and which led to the development of the large fluvial spreads of the Vosgian sandstone. Sequences 2 and 3, represented by the Vosgian sandstone units (GV1 and GV2), reflect a strong vertical aggradation of the fluvial systems, the available space (accommodation) created by the rise in base level (transgression) being largely balanced by the deposition of fluvial sediments. An important regression marks the top of Sequence 3 and was accompanied by a major regional unconformity (H) interpreted as being of tectonic origin. This unconformity could have been responsible, within the study region, for the non-presence of a regionally known sequence marking the maximum regression. This tectonic event within the middle Buntsandstein also appears to have been responsible for a modification in the configuration of the basin, and consequently of the fluvial networks. Thus sequences 4 and 5, defined in the Intermediate Beds and the Voltzia sandstone, show facies sequences

reflecting different depositional systems from those of the Vosgian sandstone. Moreover, these two sequences mainly recorded successive transgressive events which led to retrogradation of the Muschelkalk clay-carbonate lagoonal facies over the Buntsandstein continental sandstone.

In this context, the localisation of the best potential initial reservoirs was dependent on the depositional sequence and the stacking pattern of the elementary sequences, both parameters being largely controlled by tectonic events and variations in base level (tectonism and eustasy). The best potential reservoirs were initially the sandstone bars built by the large fluvial system of the Vosgian sandstone during a period of strong vertical aggradation, i.e. during the transgressive phases of sequences 2 and 3 (Fig. 24). The regressive trends and (or) the modification of the fluvial systems (related to tectonism) seem to have been responsible for a degradation in reservoir quality in the other units (presence of sedimentary discontinuities, thin sandstone bodies, development of clay facies and pedogenesis).

4. FRACTURATION OF DEEP CLASTIC RESERVOIR

Fracture characterization was based on structure typology and fracture properties including their geometry and their mineral infilling estimated macroscopically. The relation between the fracturation and the diagenetic processes is developed in chapter 5.

4.1. BASIN STRESS HISTORY

The Hercynian orogeny, characterized by a N60E orientation and the tertiary opening of the graben represent the two main geological events responsible for the actual pattern of this area. The early geological history could be deduced by integration of field data (Villemin, 1986 ; Bergerat, 1985 ; Schneider, 1984) coming from neighbouring regions of the Rhine graben (Vosges, Lotharingian Basin, Sarre-Nahe Basin, western graben border). By comparison with these regional field studies, a paleostress field reconstruction was attempted in order to propose fracture history. A summary of the successive paleostress fields (Table 1) indicates that there is a considerable scatter in indicated paleostress orientations. The two main brittle tectonic episodes which have affected this area are the Eocene compressive stage and the Oligocene distensive stage. They generated fractures which are oriented NW-SE, NNW-SSE, N-S, NNE-SSW and NE-SW (Villemin and Bergerat, 1987). Deep clastic Buntsandstein sediments have recorded successive extensional and compressional paleostress fields. From Permian until final Oligocene times, most of them are perpendicular one another suggesting that a given fracture could be easily reactivated during a new paleostress field. The resulting natural fractures pattern will be greatly induced by the effect of these major brittle stages.

4.2. TYPOLOGY OF STRUCTURES

In this section, two main structure types were analysed: (1) structures related to vertical movement occurring during lithification and (2) five types of brittle structures related to the tectonic history of the graben.

4.2.1. Early clastic dikes.

Fractures sealed with sandstone material were observed in many places of the triassic sandstones. These early structures, so-called clastic dikes, are contemporaneous of the lithification of the sandstones and are generated by subsidence movements.

These synsedimentary dikes could be interpreted as slurries of unconsolidated sand derived from undercompacted sediments which are injected into an adjacent formation.

4.2.2. Brittle structures

From core analysis, numerous structures are filled with hydrothermal products and show no evidence of movement: this type was classified as tension fissure and represents the majority of the natural fractures occurring within these deep triassic sandstones (Table 2). Few fracture planes showing vertical striation or presumed significant displacement were interpreted in terms of normal fault and fault respectively (Table 2). A rather limited number of structures was not sealed and was consequently so-called dry fissure. Around the main fractured interval, located at 1200 m depth, altered zones were observed. All these structures were created by successive tectonic brittle stages which have occurred since the deposition of Buntsandstein formation.

4.3. FRACTURE PROPERTIES VERSUS DEPTH

4.3.1. Structure density versus depth

Fractures are not distributed at random along the 410 m long core sections in EPS-1 well (Fig. 6). They are concentrated into high fracturing zones (more than 5 joints/meter) alternating with low or not fractured intervals. The average fracture density per meter is 0,85. In EPS-1 well, three main highly fractured zones could be distinguished:

- the transition between Muschelkalk formation and upper Buntsandstein (1009-1020 m), indicating the occurrence of a major fault, so called the Soultz fault (Schnaebeler, 1948);
- between 1170 and 1215 m depth, within the Vosgian sandstones, corresponding to the highest naturally fractured zone where hydrothermal deposits occur. The intensity of hydrothermal sealing suggests that this zone was probably permeable. Significant examples of open fractures were observed in this zone (Fig. 4)
- between 1360 and 1380 m depth, within the Annweiler sandstones.

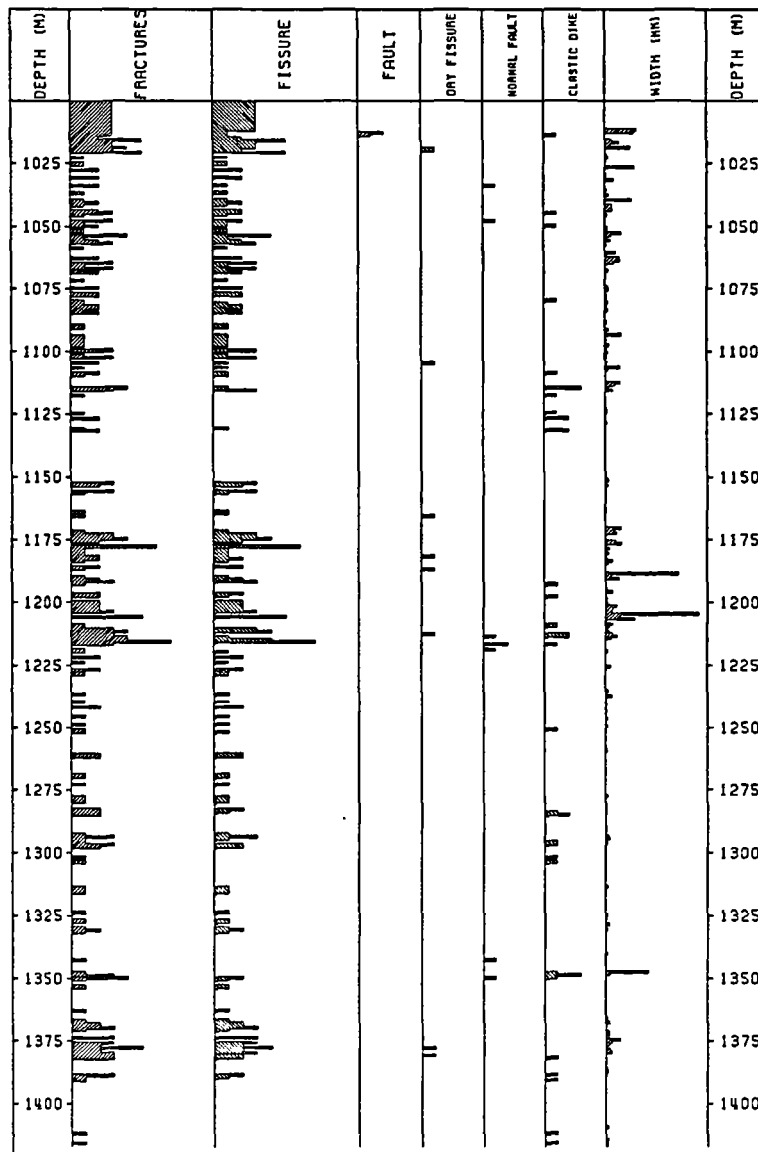


Fig. 6 - Profiles of the overall natural fractures frequency per meter and of the frequency of different types of structure (tension fissure, fault, dry fissure, normal fault, clastic dike) observed on the core section of the EPS-1 well and profile of the cumulative fracture width expressed in mm per meter.

The distribution of the tension fissure versus depth is similar to that of the whole set of data. The faults are located at the top of the Buntsandstein and correspond to the passage of the Soultz fault. The lack of the upper part of the Buntsandstein (Votzia sandstone) probably moved by this fault, confirms the importance of this major structure. Fractures without filling are preferentially located within highly fractured zones as well as microfaults showing normal striations.

The distribution of the clastic dikes is not fully dependent of the brittle structures. They are located within or outside these main fractured zones. The analysis of macroscopic fracture density, sealed width and free aperture enabled to identify three distinctive fractured intervals and to propose a hierarchy in terms of fluid circulation. The Soultz Fault location is therefore confirmed (1000m), the occurrence of a new major fault zone too (1200m) whereas the deeper fracture zone seems to be less important in terms of potential hydraulic drain.

4.3.2. Profile of cumulative fracture width

The profile of the cumulative amount of fracture width expressed in millimetres per meter of depth, is not random but fairly dependent on fracture frequency distribution (Fig. 6). When the width per meter is large, there is a large number of fracture. For instance, the maximum cumulative width (64 mm) is located between 1170 and 1215 m depth within the highest fractured zone. This relation is also observed for the fracture zone located at the top of the Buntsandstein formation (1009-1020 m). On the opposite, the deeper fracture zone (1360-1380 m) shows a low cumulative width per meter indicating that the fracture size should be rather limited.

Then, this profile could be interpreted as a function of the hydrothermal activity occurred within the fracture system and consequently a measurement of their permeability. It confirms the location of the three main fractured intervals and enables a hierarchy of their natural hydraulic behaviour.

4.3.3. Profile of fracture filling

Vertical zonation of hydrothermal minerals and organic compound which sealed natural fractures are presented in Figure 7. Nature of fillings was first recognized macroscopically on the core sections and then confirmed locally by X-ray diffraction analysis. The main hydrothermal minerals deposited within fractures in EPS-1 well are : barite, carbonates (calcite, siderite, ankerite), galena, pyrite, quartz and hematite. Organic products and oil impregnation were observed in many places. The first ones are fairly associated with mineral filling such as calcite or barite whereas the second ones impregnated fracture wall rock over centimetre scale. Their occurrences are related to the successive hydrothermal events which took place through the fracture network:

- Particles of organic matter are spatially limited to the upper unit of the Buntsandstein formation (Intermediate beds). There is no evidence of organic compounds in fracture filling in the other units of Buntsandstein except oil impregnation at 1110 m depth around fracture.
- Quartz deposits are mainly located within the main fractured zone between 1175 m and 1210 m depth.
- Barite deposits are abundant in all the sub-units of the Buntsandstein formation except in its lower part (Annweiler sandstones). At 1200 m depth, the thickest fracture filling (50 mm) is mainly composed of massive milky-coloured to pink-coloured barite.
- Calcite and siderite are abundant at the top of the Buntsandstein within a main fractured zone. Calcite deposited in fractures is abundant around 1350 to 1380 m depth where barite is rather lacking.
- Sulphides (galena, pyrite) and siliceous minerals (quartz, chalcedony ?) were mainly observed in fractures located both within the highest fractured depth intervals and the thickest hydrothermal deposit width (1170-1215 m). Bleached zones seem closely related to pyrite occurrences.
- Hematite only occurs at proximity of the granitic surface. Clastic fillings are located in early fractures intersecting all the Buntsandstein unit. They occur both within highest or lowest fractured zones. Dry fissures seem closely associated to high fractured zones.

A detailed fluid inclusion study of the primary or secondary minerals (quartz, barite) sampled at different depth in the triassic sandstones and in the granite was carried out by Dubois et al. (in press).

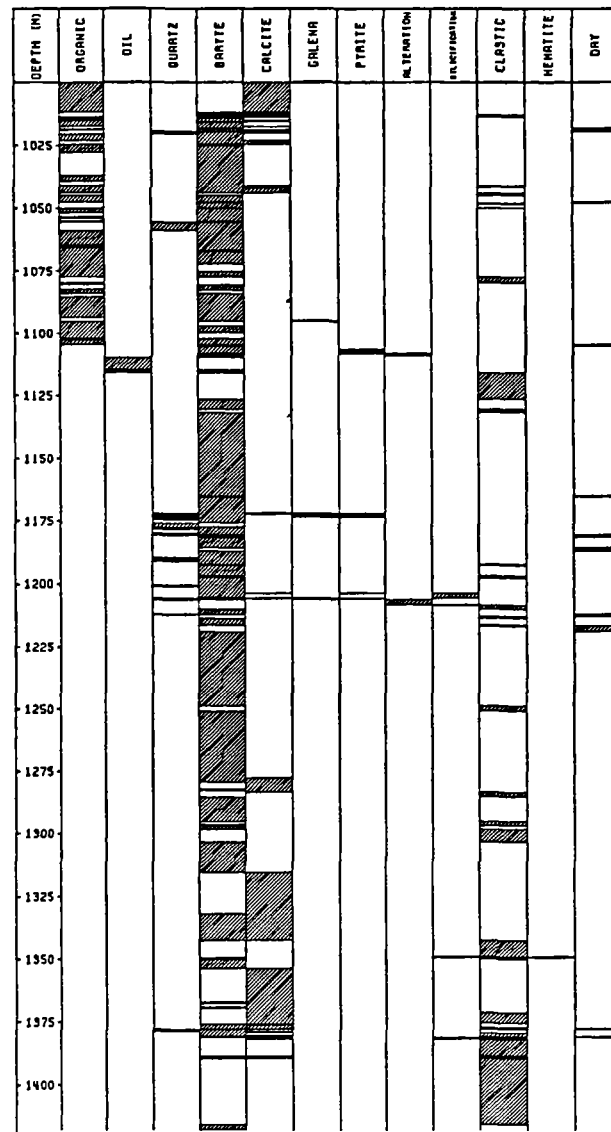


Fig. 7 - Profiles of the various hydrothermal or organic fracture filling versus depth observed on the core section of the EPS-1 well.

4.4. FRACTURE CHARACTERIZATION

4.4.1. Geometry of the natural fracture system

The preferential fracture striking orientation is N170E (Fig. 8). This direction corresponds to two conjugated fracture sets steeply dipping eastward and westward. Three secondary fracture peaks occur and are characterized by an orientation N20E, N60E and N140E.

The histogram of raw fracture dips shows that fracture are highly dipping but with only few subvertical data due to vertical sampling bias (Fig. 9A). After correction of borehole trajectory applied to the whole set of data (Terzaghi, 1965), the fracture dips distribution shows a positive exponential law (Fig. 9B). Therefore, the fractures intersecting Buntsandstein sandstones are characterized by high dipping values.

Stereographic projection of all the data gives the attitude of the fracture system which is purely conjugated and strikes N170E with a dip of 75W and 75E (Fig. 10A, 10B). Tension fissures show a similar fracture attitude with a prominent submeridian fracture set (Table 3). Clastic dikes are characterized by a preferential orientation N60E and a secondary set oriented N170E (Fig. 10C). Normal faults, dry fissures and alteration limits are striking N-S to NW-SE whereas fault structures are striking NE-SW (Table 3).

Nine brittle natural structures present a composite fracture filling including clastic sediment and hydrothermal deposit (calcite, barite). The different origins of these fillings suggest that these discontinuities correspond to early clastic dikes which were reactivated later on. Moreover, their average striking orientation which is N-S, is consistent with a reworking due to the Oligocene extensional regime.

Clastic dikes characterize early stages of extensional regimes occurring during the compaction of Buntsandstein formation. If we consider these synsedimentary structures as tension fissures, the orientation of the minimum horizontal paleostress which has generated them, should be perpendicular to their strike azimuth and gives the direction of extension.

Therefore, two principal stages of early extension could be deduced from the orientation of clastic dike population. The principal one is oriented N150E, corresponding to N60E oriented dikes (hercynian direction) and shows no evidence of reworking. The secondary one is oriented N80E, corresponding to N170E dikes and was probably reactivated during Rhine graben formation.

4.4.2. Fracture orientation with depth

Vertical distribution of fracture dip direction shows three distinctive depth fractured intervals (Fig. 11A). The top of Buntsandstein (1008-1080 m) where dip directions are rather scattered over 360 with two maximum between 40 and 280-300. Fracture orientation is more stable deeper. Between 1160 and 1200 m and around 1380 m depth, two sets of dip direction occur and are oriented 80 to 100 and 250-270.

Distribution of fracture dip with depth is stable (Fig. 11B). Fractured zones are characterized by high dipping value ranging between 55 and 85°.

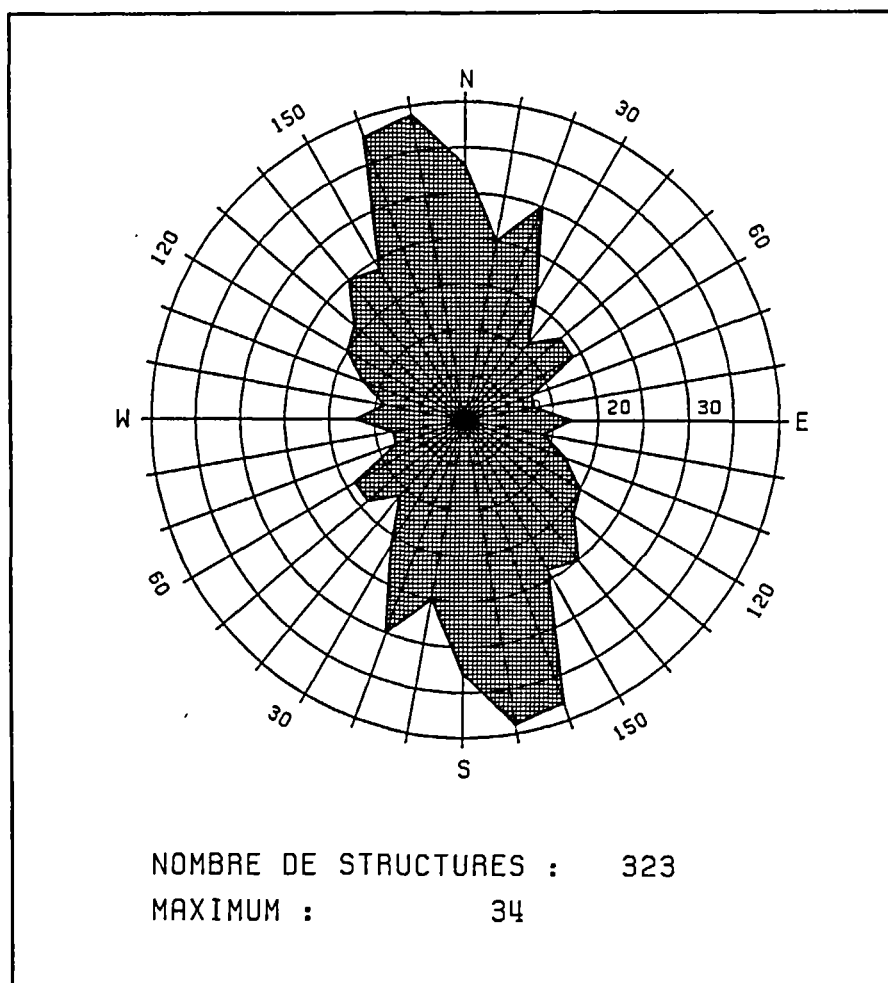


Fig. 8 - Rose diagram of strike azimuth of overall fracture population in EPS-1 well (N = 322).

4.4.3. Fracture width

Most of natural fractures observed on core sections are sealed by hydrothermal and/or organic materials. The width of these deposits ranges between 0 to 5 centimetre-thick. Fracture width population describes a negative exponential law (Fig. 12A). Fracture width ranging between 0.1 and 3 mm dominates and represents about 95 % of the total amount of fractures with an average value of about 2mm. The thickest fractures are sealed by euhedral barite, galena, pyrite and geodic quartz and are located within highly fractured depth intervals. The cumulative fracture width is 710mm for the whole set of data.

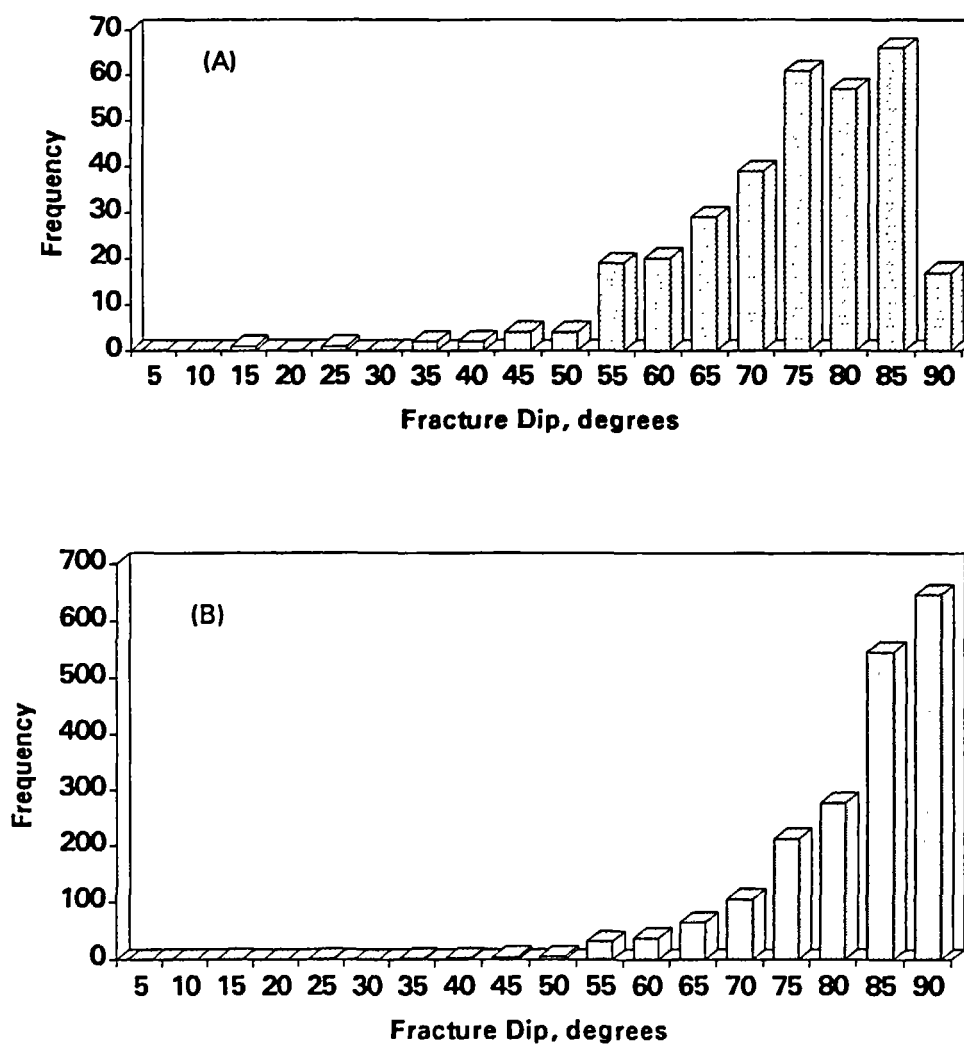


Fig. 9 - Frequency histograms of fracture dips between 0 and 90 for all the natural fracture population (N= 322 data) observed on the EPS-1 core sections.
(A) Uncorrected dip values.
(B) Corrected dip values according to the method of Terzaghi (1965).

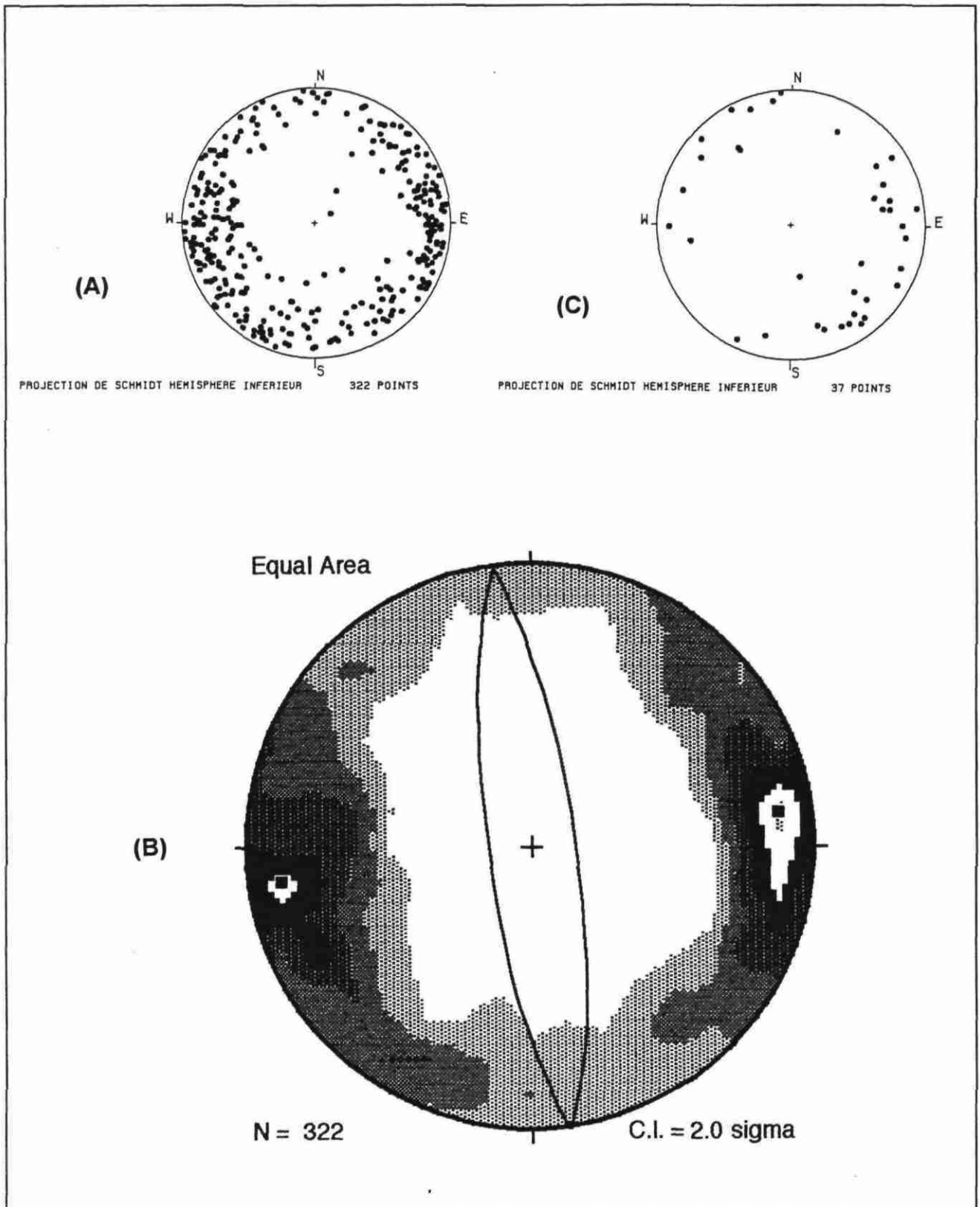


Fig. 10 - Lower hemisphere schmidt projection of pole of natural fractures and Kamb contour of pole densities in Buntsandstein of the EPS-1 well (1008 - 1418 m) from core analysis.
 A - overall population
 B - density plot of overall population (N= 322 data)
 C - Clastic dike (N= 37 data)

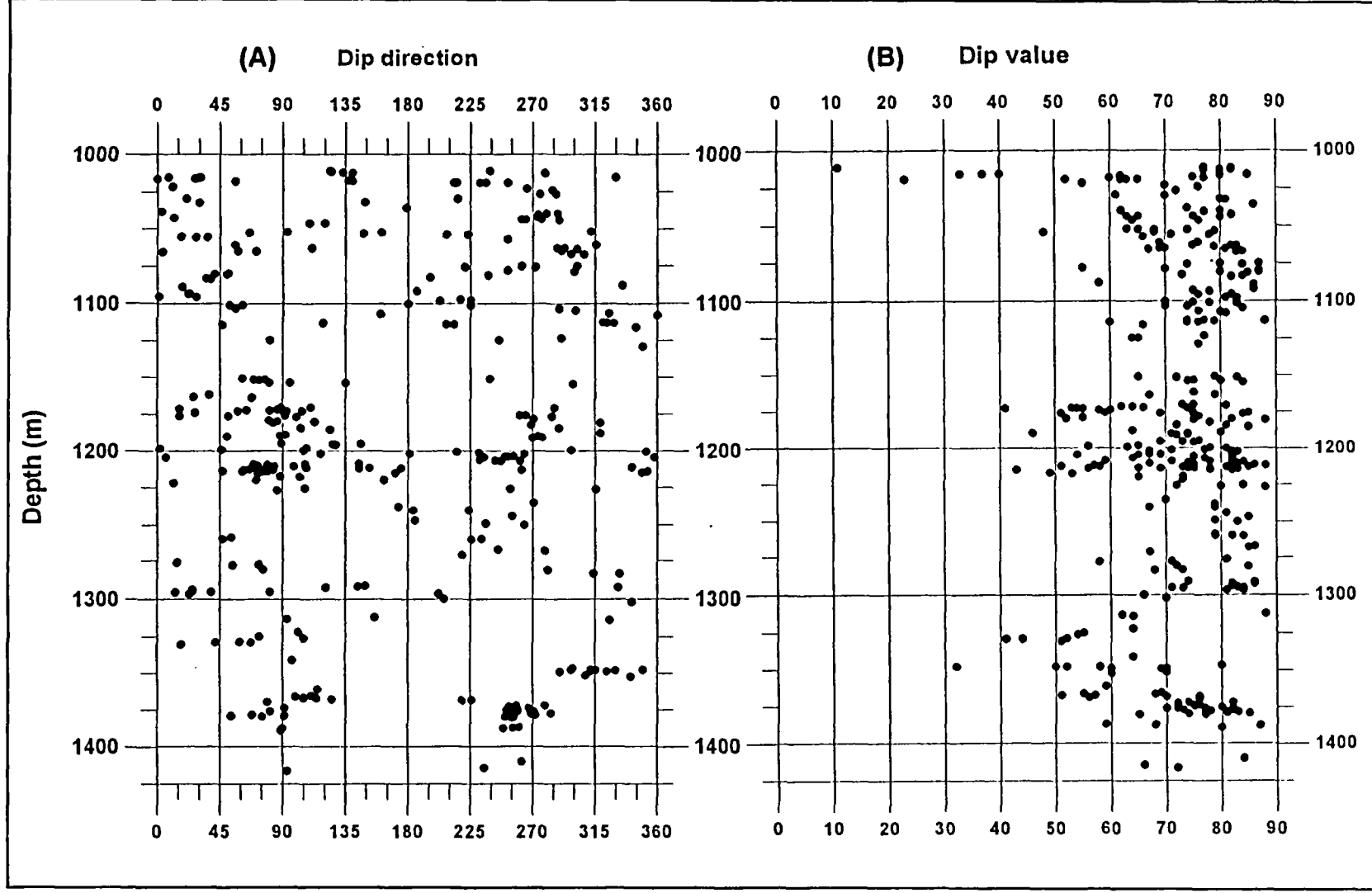


Fig. 11 - Profiles of macroscopic natural fractures observed in the core section of the EPS-1 well.

A - Fracture dip direction
B - Fracture dip

4.4.4. Fracture free aperture

Natural fractures observed on core section show not only significant hydrothermal filling width but also a free aperture or evidence of free aperture in their central part. This free aperture doesn't exactly correspond to regular planar structure. It could be defined as a void within the fracture filling, i.e. a residual aperture. This void is controlled by the geometrical characteristics of secondary barite which crystallises with entangled tablet shapes.

Scarce examples of geodic barite or geodic quartz occur with a rather regular free aperture plane. It was approximately measured due to its lower size. 36 % of the amount of fracture show a free aperture (Fig. 12B). It ranges between 0,1 and 8 mm but its average magnitude is 1 mm. The cumulative free aperture is 145 mm for the whole set of data.

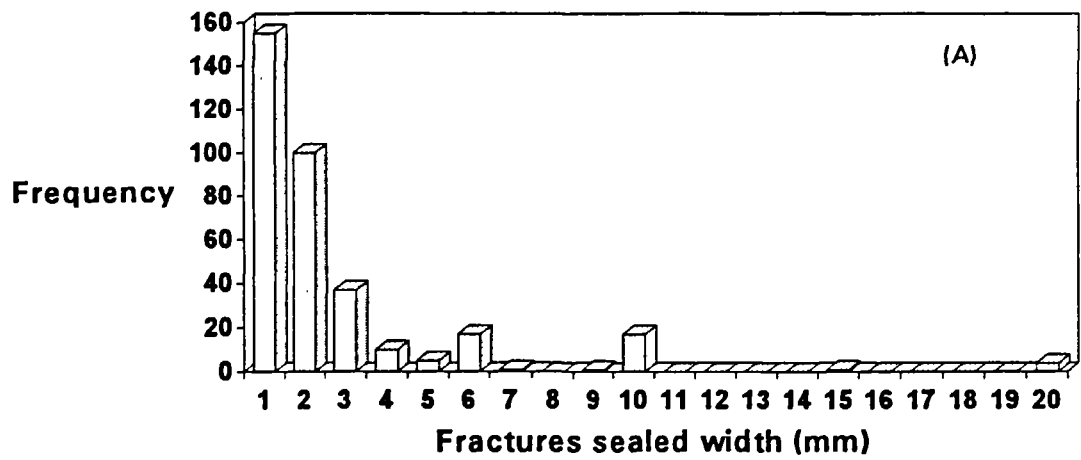
Distribution of free aperture of fracture width depth (Fig. 12C) shows a close relation with fracture frequency. The highest free aperture values are located within the highest fractured zones and reciprocally.

The ratio between the cumulative free aperture and the cumulative fracture width could be considered as a fracture permeability indicator. This ratio gives a value of 0.20 for the entire population of fracture.

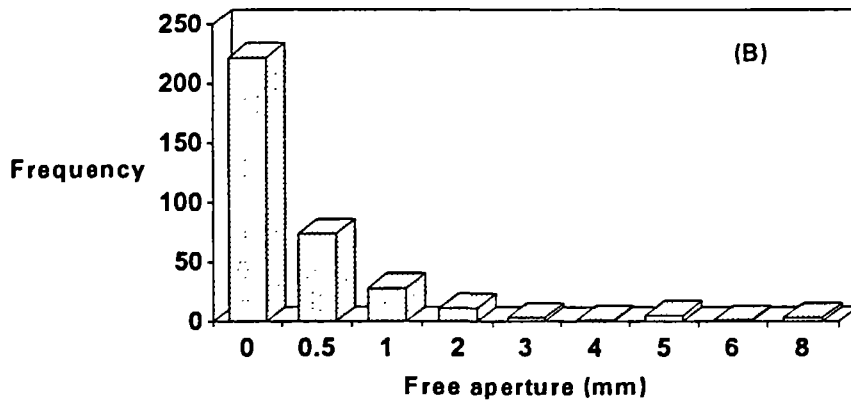
4.5. INFLUENCE OF TECTONIC FEATURES ON THE JOINT NETWORK FOR EVALUATION OF CLASTIC GEOTHERMAL RESERVOIR

Clustered organisation of natural fractures is related to the successive tectonic regimes affecting this area. The most important of them was the Oligocene extension which created the Rhine graben and permits the formation of normal faulting system. Therefore, the occurrence of these fractures generated by an extensional regime would be favourable for fluid circulations.

In terms of orientation, natural fractures show a pure conjugated pattern striking N170E with a dip of 75W and E emphasizing the role of the E-W Oligocene distensive stage. This general submeridian orientation was deduced from core analyses in EPS-1 well over 410 m length and from borehole imagery in 4550 and GPK-1 wells. The high dipping of the fractures suggests that they would be favourable to fluid transfer.



EPS-1 well, natural fractures



EPS -1 well, natural fractures

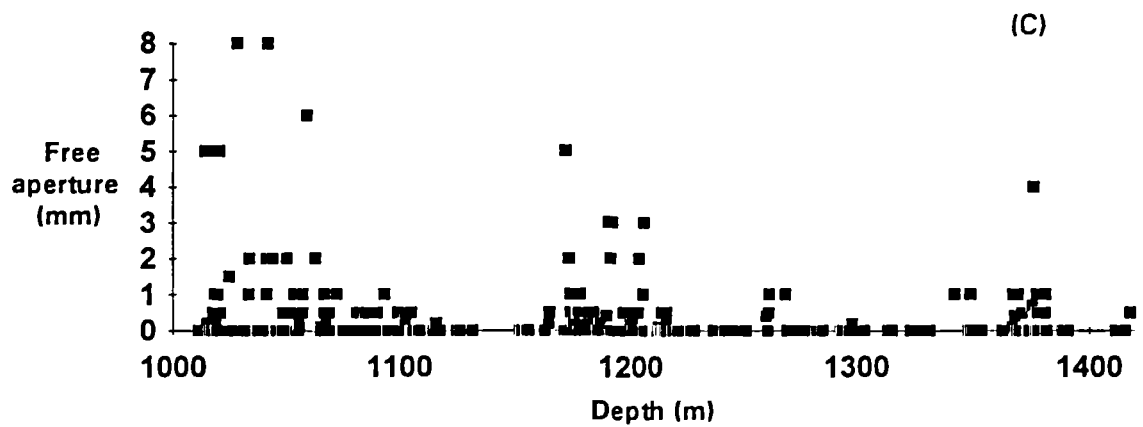


Fig. 12 - Frequency histograms of fracture sealed width (A), of fracture free aperture (B) and profile of fracture free aperture versus depth (C) measured on the core sections of EPS-1 well.

The secondary fracture set orientations which are N20E and N140E are consistent with the Eocene compressive stage. This brittle tectonic phase is one of the most important in this area. The N60E orientation which characterizes the clastic dikes corresponds to a Buntsandstein synsedimentary extension.

Within the graben, the general compartmenting of the sediments was induced by the major normal faults which present a significant vertical offset. The Sultz fault which is antithetic to the border Rhenan fault presents an offset greater than 500 m. However, it was difficult to get accurate information about the offset of macroscopic fractures only from core or borehole data.

The clastic veins or the synsedimentary normal fractures are mainly sealed by early lithic sediments showing a clastic composition (sandstone). Therefore, these structures do not induce a strong anisotropy within the Buntsandstein. They constitute minor heterogeneity and do not really influence the reservoir properties in terms of permeability. Occurrences of organic compounds in fracture planes suggest migrations from Pechelbronn oil fields.

Most of macroscopic fractures are fully filled with hydrothermal or organic compounds. Moreover, within the highly fractured zone located at 1200 m depth, the surrounding of this fault was affected by the precipitation of silica and barite. This wall rock effect is visible within 1 or 2 m. Now, this fault acts as an impervious barrier and represents a tight limit between two major blocks within the Buntsandstein formation. Then, fault sealing reduces the reservoir quality within the cementation zone which is roughly developed paralleling to the fault.

No evidence of natural water outflow was detected in EPS-1 well even within highly fractured zones. However, in two closer boreholes, 4550 and GPK-1 wells, an outflow of hot water or fluid losses were alternatively observed during the drilling of these major fault zones. From a hydraulic point of view, the natural behaviour of a given major fault is therefore strongly heterogeneous.

Although numerous macroscopic fractures present a free aperture, its influence seems rather limited for fluid conduction. In fact, this free aperture does not constitute a clear open joint but is due to a partial sealing of fracture plane permitting a discontinuous or irregular void within the hydrothermal filling itself.

Age	Paleostress field data	Orientation of main brittle structures	Intensity of tectonic event
Upper Miocene to Actual	NW-SE compressive regime	N-S reactivated sinistral shears	minor
Miocene	NE-SW compressive regime	N-S reactivated dextral shears and E-W to ESE-WNW reactivated sinistral shears	minor
Oligocene	E-W distensive regime	N-S to NNE-SSW normal faults	major
Eocene	N-S compressive regime	NW-SE dextral faults and NE-SW, NNE-SSW to N-S sinistral faults NNW-SSE to NNE-SSW tension fissures	major
Trias to late Jurassic	E-W distensive regime	N-S, NNE-SSW, NE-SW and NW-SE normal faults	minor
Permian to early triassic times	N-S to NNE-SSW distensive regime	E-W normal faults	intermediate

Table 1 - Successive paleostress fields and associated brittle structures affecting the Upper Rhine graben and its surrounding area (Bergerat, 1985 ; Schneider, 1984 ; Villemin, 1986 ; Villemin and Bergerat, 1987)

Structure types	Recorded	Oriented
Tension fissure	284	262
Normal fault with striae	8	8
Clastic dike	41	37
Fissure without filling	8	8
Alteration limit	4	4
Fault	3	3
Total	348	322

Table 2 - Amount of different types of macroscopic structures recorded on the Buntsandstein core section of the EPS-1 well and successfully oriented.

Type	Number of data	Principal fracture set	
All structures	322	N170E	75W,E
Tension fissure	262	N170E	80W,E
Clastic dike	37	N060E	75S,N
Normal fault	8	N180E	50E
Fault	3	N040E	80E
Dry fissure	8	N160E	60E
Alteration limit	4	N150E	75W

Table 3 - Structural data orientation within Buntsandstein formation

5. PETROGRAPHY AND DIAGENESIS

The triassic sediment of EPS-1 borehole underwent many diagenetic events characterized by mineral precipitation and dissolution, in cement and fractures and by replacement of primary minerals (Fig. 13). The initial sediment underwent an early diagenesis, controlled by the initial sediment and fluids composition, and early events such as pedogenesis. Compaction and burial diagenesis then induced further transformations. Tectonic events and associated hydrothermalism induced an important fluid circulation and mineral deposition in fractures and in cement of wall-rock sediments.

5.1. INITIAL SEDIMENT COMPOSITION

The different lithostratigraphic units of the Buntsandstein formation are dominantly composed of a lithic and feldspathic sandstone. The amount of clay is a key for the distinction between lower unit (Annweiler sandstone) and upper unit (Intermediate Beds).

The initial sandstones sequences (plate 1: photo 1) contained 20 to 40 % of quartz in average with a maximum of 60 % at the top of the Vosgian Sandstone, associated to an initial higher porosity and permeability. Feldspar content, essentially potassic, varied between 5 and 10 %. Those minerals are presently strongly altered. It is very likely that this alteration started prior to deposition and increased by diagenetic processes.

The lithoclastic content of those sandstones varies between 10 and 20%. Volcanic, granitic and quartzitic clasts are present in equivalent amounts (plate1: photo 2). Clayish intraclasts are present in the lower part of some sandstone sequences, witnessing reworking of underlying or proximal clay beds. Detritic micas are observed in the upper unit (Intermediate Beds). Heavy minerals (essentially tourmaline and zircon, belonging to the sand fraction in size) are commonly present in a rate of 1%.

The fine fraction of sandstone facies is composite : clay content (illite and illite-smectite) varies between an average of 15 to 20 % in the Annweiler sandstone to 5 % in the Vosgian Sandstone (plate1: photo 3). A fine fraction, opaque to optical microscopy and intricated with clays ribbon, is composed of iron oxides (hematite) and hydroxides and apatite. This last fraction amounts to an average of 5% in the cement of sandstones.

The grain size distribution, clay content, and geometry of porous and non-porous bodies shows that initial reservoir quality can be considered as poor in the Annweiler sandstone and Intermediate Beds and good to very good in the Vosgian sandstone. The initial porosity at the scale of sandstone bodies (metric to plurimetric) could be globally considered as homogeneous. But the variability of grain size, associated to cross-bedding organisation, especially in the Vosgian sandstone, induced a variability at a centimetric scale of both initial porosity and clay content and as a consequence, preferential drains for diagenetic fluids.

5.2. DIAGENESIS

5.2.1. Pedogenic diagenesis

Few early diagenetic events are recorded in the EPS-1 triassic sediments. In the Annweiler Sandstone and basal Vosgian sandstone, they are mainly pointed out by sparitic nodules in the cement of sandstones and layers showing a rhomboedric zoned calcidolosparite, underlining pedogenetic features, reaching 25% within an argillaceous, micritic and ferriferous matrix.

We observed 5% of sparitic nodules in the cement; these nodules are dominantly calcisparitic with a relatively high content in iron and manganese; they also contain patches of siderite. The primary nodules were likely to

have been micritic intraclasts reworking an underlying or proximal pedogenetic level. Calcisparitisation would be a later phenomena linked to burial diagenesis and siderite patches would be synchronous to fracture fillings of siderite. In fact, pedogenesis did not modify initial reservoir quality.

5.2.2. Early burial diagenesis

Early burial diagenesis is likely responsible for genesis of sandstone filled fractures, so called "clastic dikes" (plate1: photo 4) injected from an adjacent sequence of sediments, within an underconsolidated material.

Burial diagenesis can be characterised by sparitisation of pedogenetic carbonates (plate 2: photo 1). Compaction and burial also lead in sandstone facies to a rearrangement of detritic grains and features of pressure and dissolution (plate 2: photo 2). This process result in puncture and dissolution of the softer mineral or clast, or in an elongation of the grains when pressure acts between minerals or clasts of equivalent hardness.

As described by Sizun Jeanette (1995), the modification of quartz volume due to pressure and dissolution ranges between 0 and 5 % in sandstone facies. In the upper part of Vosgian sandstones, the pressure and dissolution features are absent or few. Small and irregular rings of quartz authigenesis are observed at quartz grains junctions, consecutive to a proximal dissolution; they range between 1 and 5 % of volume increase. Thin rings of feldspathic authigenesis are also observed on detrital feldspar, inducing an increase of volume between 1 and 5 %. Feldspar authigenesis is more systematically present in the Intermediate Beds.

The evolution of reservoir quality related to burial diagenesis shows a decrease of intergranular porosity between 1 and 5% of the volume, linked to grain rearrangement, and associated authigenesis,

5.2.3. Impact of late burial and tectonism on diagenesis

The first mineral transformation observed in the wall rock are feldspar alteration and clay recrystallization (Fig. 13). They are related to deep burial and/or hydrothermalism. Feldspar alteration started very likely before deposition and compaction of the sediment (plate 2: photo 3 and 4). It is increased by diagenetic processes. This secondary alteration occurred after the formation of the ring of authigenesis. Dissolution acted on the primary alteration products and destabilized the detritic grain, preserving the authigenic ring and the grain shape and frame. Alteration can reach 5 to 7 % of the total volume of sediment, with a nearly complete dissolution of the grain, residual skeleton, and intragranular porosity.

The heterogeneity of grain size is associated with a differential feldspar alteration. Feldspars in fine grain layers, rich in clay, with dominant micro-porosity, are more strongly altered than coarse grained layers with macro-porosity. This can be associated with a longer time of residence of the fluid responsible for feldspar dissolution. Feldspar alteration creates a large volume of secondary porosity which is however likely to be inefficient, due to its morphology in narrow channels, easily plugged by by-product particles.

In the Buntsandstein sandstones, clays are mainly illite and illite-smectite mixed-layers, with locally a small amount of chlorite. Two textural phases have been observed: plates and lattices (Cassagnabère, 1993; Vinchon et al., 1993). They have a similar composition and a centripetal organisation in regard to the intergranular porosity. From edge to centre, we observe small size plates associated with quartz authigenesis on the edge of detritic grains, then a secondary plate-shape phase, organised in a honeycomb net. A third phase of long lattices give to the porosity walls a "hairy" aspect (plate2: photo 4).

If it is very likely that clay is partly inherited and its present texture implies diagenetic processes, linked to burial and/or tectonic events, These processes induced recrystallisation of the primary phase and authigenesis. Sandstones sedimentation conditions suggest that the grains were deposited with a clay coating recrystallised in the first phase, at the same time as quartz authigenesis (burial conditions). No arguments can be given, at this stage of the study, to choose between a complete authigenesis (burial and/or tectonic events) of the honeycomb organised plates and associated hairy lattices, or a partial heritage as detritic matrix. Distribution of porosity is

tightly linked to the texture of clay, inducing a micro-porosity on the edge of intragranular spaces and channels. Clay recrystallisation maintains a micro-porosity, which, because of its morphology, is inefficient and would rather decrease the reservoir quality;

Late burial is responsible for feldspar alteration and for clay recrystallisation and tectonic events are responsible for depositions in fractures. Tectonically induced hydrothermal circulations are known in the underlying granite and brine is observed in other wells and could be also associated with those mineralisations. However, no petrographic argument exists in minerals deposits of the EPS-1 Buntsandstein to suggest the effect of recent circulations on mineralisations.

When the first mineral phases are related to deep burial and/or hydrothermalism linked with tectonics, the further mineral phases, encountered both in fractures and sandstone cement, are then directly linked with tectonic events (Fig. 13).

A silicification, more or less developed, is observed at the wall of all fractures, with an automorphic to petaloid quartz shape (plate 3: photo 1 and 2). Wide rings of quartz authigenesis are also observed (plate 2: photo 7), more specifically in coarser and cleaner sandstone layers. Those authigenic rings act as preferential drains, within the Vosgian sandstones. They can lead to a increase of the quartz volume of 1 to 5%. The involved volume, the development of the quartz in the better primary drains, and the cristallisation at the fracture wall suggest a tectonic diagenesis, associated with hydrothermal circulations. Nevertheless, in most samples, it is difficult to differentiate this later phase from earlier silicifications.

A peculiar siliceous phase is encountered in the surrounding of the 1205 m fault. Associated to the above quoted automorphic to petaloid quartz phase in fractures, a microquartzite silicification is developed in the wall-rock (plate 2: photo 6; plate 3: photo 1). In the vicinity of the fault, the wall-rock sandstone is "digested", leaving a few residual quartz in a microquartzitic matrix. In a range of 5 to 10 meters above and under the fault, the phenomena is less important and microquartz is present as cement. This microquartz silicification can be attributed to fluid circulations in the fractures.

The microquartz silicification results in an insignificant porosity, and the formation of a barrier level for further diagenetic fluid circulation. The underlying part of Vosgian sandstone seems to have been protected from further fluid circulation, until the 1205 m fault and associated fractures are reactivated and opened to baritic fluids.

Scarce sulphurs (pyrite and galena) are observed, in zones of developed silicification, consecutive to this phase.

Silicification is followed in fracture fillings by the deposition of carbonates of siderite type (plate3: photo 2 and 3), whose rhomboedric texture is dependant of the free space for mineralisation. This mineralisation is sporadically observed in the fractures, more frequent in the upper units and top of Vosgian sandstone. A little echo of this fracture mineralisation is encountered in the sediment. In Annweiler sandstones, pedogenic calcite is replaced by siderite (plate2: photo1), that could also result of burial diagenesis.

The next filling of barite and associated automorphic quartz is observed in all fractures (plate 3: photo 4), where it has a poikilitic texture on former quartz and sulphurs and on siderite. It is also encountered in the cement of sandstones, more specifically in clean and coarse layers of Upper Vosgian sandstones and basal Intermediate Beds, where quartz and barite can necrose the residual porosity (plate 3: photo 5). It implies an important volume of mineralisation.

In specific levels, the baritic phase underwent a partial dissolution and the associated automorphic quartz in the cement are the clue which indicates a former presence of barite (plate 2: photo 7). Dissolution of barite is observed in cement of sandstones at the top of Vosgian Sandstone and in the 15 m beneath the 1205 m silicified fault. This dissolution induced a secondary porosity which is partly responsible for a better permeability at present in those two zones. This dissolution event can be recent. The last observed filling is

made of organic matter of tellinite type, and is limited to the fractured zone of Intermediate Beds and the very residual porosity of coarse sandstone. A Rock Eval analysis indicates a migrated bitumen, likely associated with the oil impregnation at the top of the Vosgian Sandstones.

Mineralisations linked with fractures fill have different impacts on reservoir quality, depending of their diffusion through the wall rock. The silicification at the wall of fractures, considerably decreased the intergranular porosity of coarse grained sandstone bed and created, by digestion of the wallrock on a short distance, a non porous barrier, that preserved the underlying reservoir from further fluids circulation. This protection is effective from 1205 to 1270 m; a clay bed of 5 m acts as the bottom-wall non porous barrier. The siderite, limited to fractures, has practically no impact on reservoir quality, if no impact at all. The tectonic event associated to barite mineralisation reactivated the 1205 m fault with a circulation of baritic fluid on a short distance in the underlying reservoir. Then, deposition of barite and associated quartz temporarily decreased the intergranular and fracture porosities. Barite dissolution partially restored the porosity when the deposition of organic matter reduced the intergranular and fracture porosities of upper reservoirs.

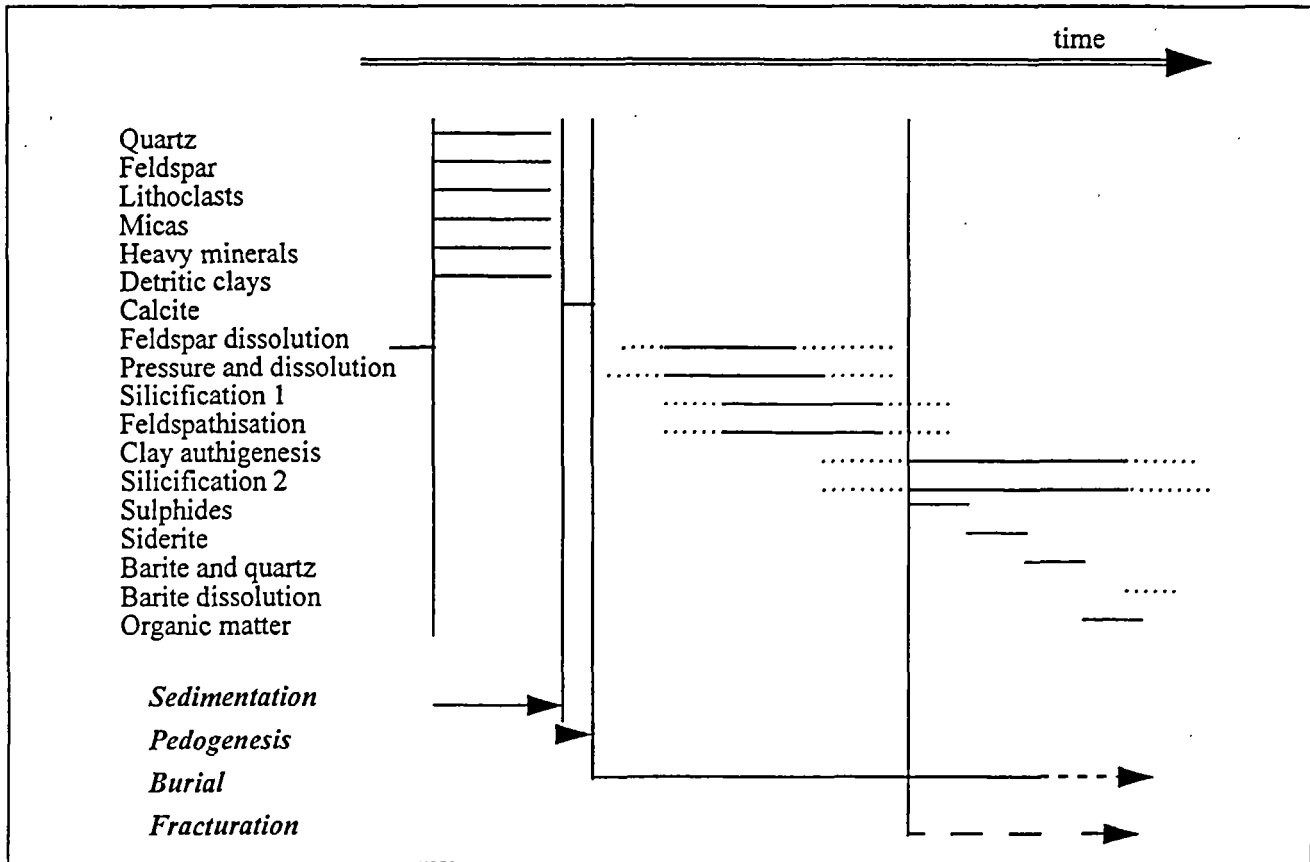


Fig. 13 - Main diagenetic phases observed in the Buntsandstein sandstones of the EPS-1 well

6. PETROPHYSICAL PARAMETERS

Porosity and permeability were measured at well scale and core scale:

- sonic porosity log
- gamma-density log (Dumas et Belpaume, 1991)
- mercury porosimetry
- gas permeability on cores

The porosity and permeability vs. depth are presented in a synthetic log (Fig. 23). At well scale, sonic porosity, gamma-density-derived porosity and mercury-porosimetry-derived porosity show a similar trend.

6.1. POROSITY AND PORE SPACE

The plot of sonic porosity vs. gamma-density-derived porosity for 392 points (one per meter) shows a relative dispersion (Fig. 14). It can be explained by the different sampling rates of measurement for the two methods (5 mm for gamma-density and 15 cm for sonic log) and by the empirical character of porosity estimation laws. A third reason is that sonic porosity is representative of the area around the well when gamma-density-derived porosity is representative of the area inside the well. It suggests horizontal heterogeneity at metric scale.

Porosity, in terms of optical microscopy, underlined by coloured resin, is composed of free intergranular spaces between grains, with an average size of 200 to 300 μm ("optical macro-porosity") and micro spaces intricated between fine particles ("optical micro-porosity"). Pre-deposition feldspar alteration induced an intragranular porosity, more or less occupied by micro particles of clays or carbonates.

For the 67 Buntsandstein samples, mercury-porosimetry-derived porosity was compared with gamma-density-derived porosity which is more representative of the core plug. As the gamma-density is measured every 5 mm and the plug has a diameter of 4 cm, the gamma-density-derived porosity at core plug scale is a mean of 9 values. Gamma-density-derived porosity is often greater than mercury-porosimetry-derived porosity (Fig. 15) which can be explained by a slight over-estimation of sandstone density. The correlation is low and can be explained by the difference between splinters and plug sizes. Even if low, the correlation remains reasonable and confirms the validity of mercury porosimetry for reservoir analysis (Melas and Friedman, 1992).

The capillary pressure curves derived from mercury porosimetry are very different for the set of Buntsandstein samples which indicates a large heterogeneity of the porous network (Fig. 16). The capillary pressure data allow to determine parameters like total porosity (Φ_t), effective porosity, withdrawal efficiency (W_e), macro and micro-porosity (Φ_M and Φ_m), pore-throat size distribution (PTD) and maximum ratio of capillary pressure and percent bulk saturation ($(S_v/P_c)_A$).

Withdrawal efficiency (W_e) is controlled by pore geometry and is defined as the ratio of the mercury saturation in the sample at minimum pressure after pressure is reduced (here to 0.4 bar) to the saturation at maximum pressure (here, 2000 bars) (Vavra et al., 1992).

$$W_e = \frac{S_{\max} - S_i}{S_{\max}} 100\%$$

The distinction between macro and micro-porosity is arbitrary and there corresponds respectively to the volume of mercury which penetrates the sample by applying a pressure of 1 bar and to the volume which penetrates the sample by increasing the pressure up to 2000 bars. PTD is a measure of the sorting of pore throats :

$$PTD = \frac{(3rd\ quartile\ pressure)^{1/2}}{(1st\ quartile\ pressure)^{1/2}}$$

where 3rd quartile is the capillary pressure at a mercury saturation of 75 % and 1st quartile pressure is the capillary pressure at a mercury saturation of 25 %. The highest values of PTD correspond to a large distribution of pore throat sizes and a value closer by unit corresponds to a small range of pore throat sizes. $(S_b/P_c)_A$ is derived from interpretation of the mercury saturation and capillary pressure data by Swanson (1981) which shows that this parameter can be correlated to the permeability.

The minimum, maximum, average and standard deviation values for these parameters are presented in Table 4.

	Φ_t (%)	W_c (%)	Φ_M (%)	Φ_m (%)	PTD	$(S_b/P_c)_A$
average	13.3	19.6	2.8	10.6	3.8	2.9
maximum	20.2	35	10.8	17.5	7.3	15.1
minimum	2.6	9	0.4	2.2	1.8	0.4
standard deviation	3.4	6.2	2.3	2.8	1.2	2.8

Table 4 - Parameters derived from mercury porosimetry

The porosity values are much higher in Vosgian sandstones (average of 13.6% for upper and 14.8% for lower Vosgian sandstones) than in Intermediate Beds (average of 11.1 %) and Annweiler sandstones (average of 10.6%). The macro-porosity is very low in Annweiler sandstones (< 1 %), low in Intermediate Beds and variable in Vosgian sandstones (from 0.8 to 10.7 %).

Withdrawal efficiency is low, indicating there is a large amount of dead-end pores and large pores connected by small throats. The withdrawal efficiency tends to decrease when porosity increases (Fig. 17), then a positive relationship is generally reported (Melas and Friedman, 1992). It suggests a low degree of connectivity at medium and high porosity.

PTD ranges between 2 and 7 which indicates a complex porous network. The intermediate Beds, which are the most heterogeneous, show the largest variation of PTD. This complexity is emphasised by the fact that PTD increases with porosity (Fig. 18) and with macro-porosity. This trend reduces the capacity to be a good reservoir rock which is characterised by a high porosity and a low PTD (Melas and Friedman, 1992).

The mercury porosity spectra show four types of pore throat distribution: (i) a unimodal distribution with only micro-porosity which is founded in Intermediate Beds and Vosgian sandstones with PTD between 2 and 4, (ii) a bimodal distribution with a micro-porosity pike and a macro-porosity pike which is founded only in Vosgian sandstones with PTD between 3 and 6, (iii) a bimodal distribution with two micro-porosity pikes more or less marked, which is founded in Annweiler sandstones with PTD of about 3 and (iv) a trimodal distribution with two micro-porosity pikes and one macro-porosity pike which is founded only in Intermediate Beds and upper Vosgian sandstones with the highest PTD values. These types of distribution are directly visible with the form of capillary pressure curves which show one, two or three inflexion points (Fig. 16).

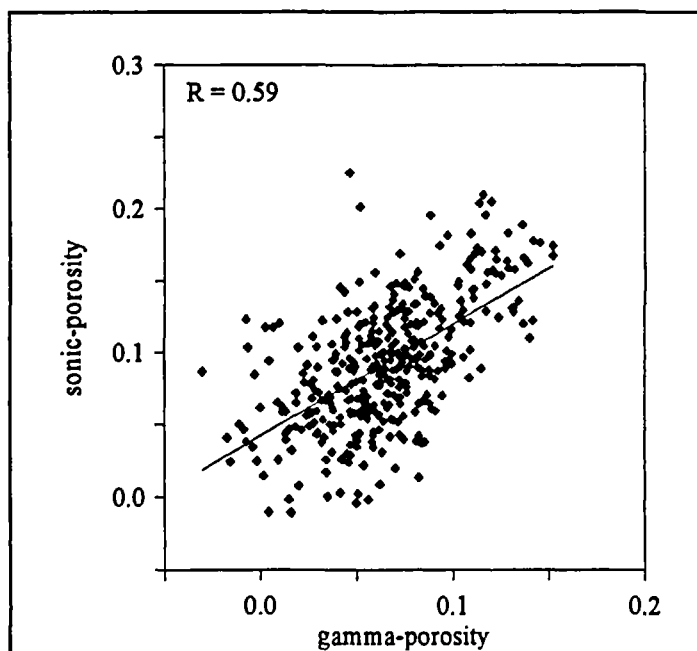


Fig. 14 - Plot of sonic-log-derived porosity vs. gamma-density-derived porosity

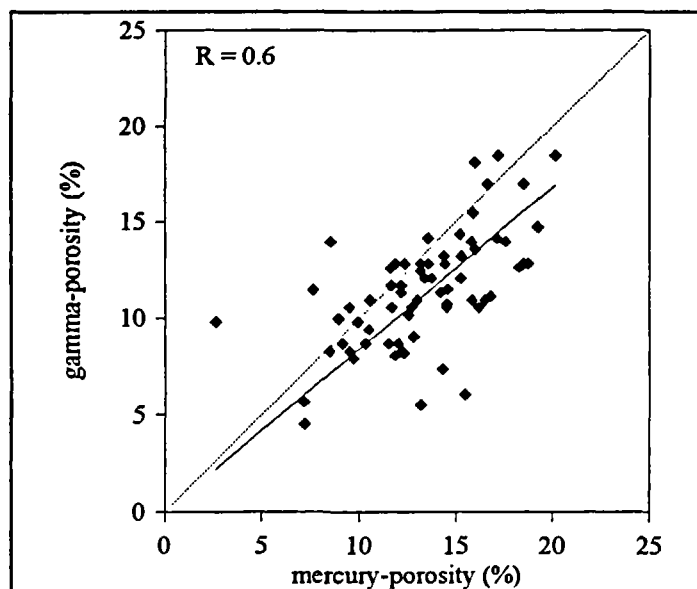


Fig. 15 - Plot of mercury-porosimetry-derived porosity vs. gamma-density-derived porosity

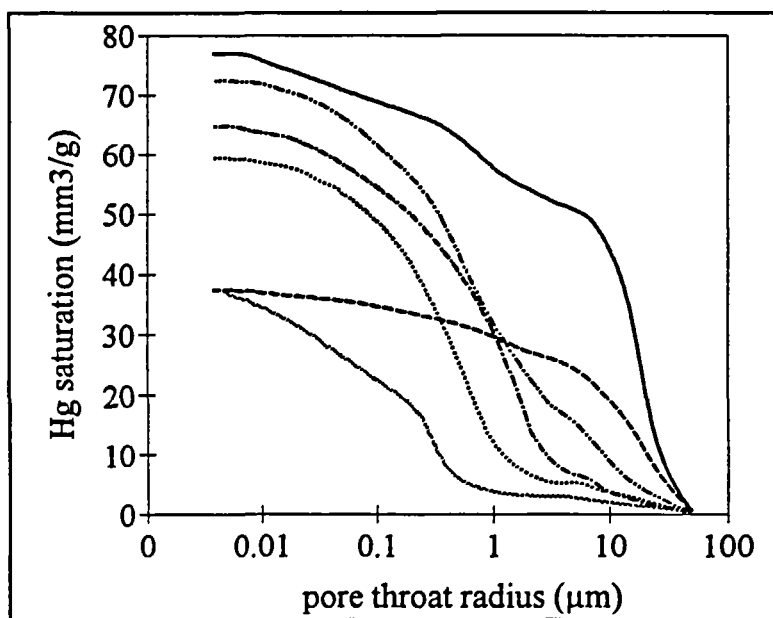


Fig. 16 - Capillary pressure curves for 6 samples of EPS-1 sandstones

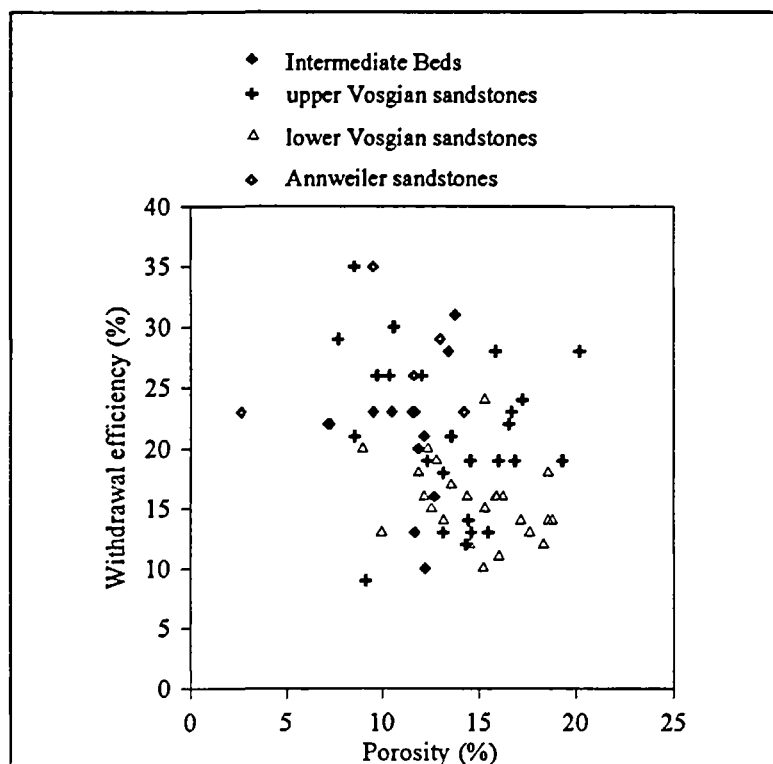


Fig. 17 - Withdrawal efficiency vs. porosity for the four main Buntsandstein levels

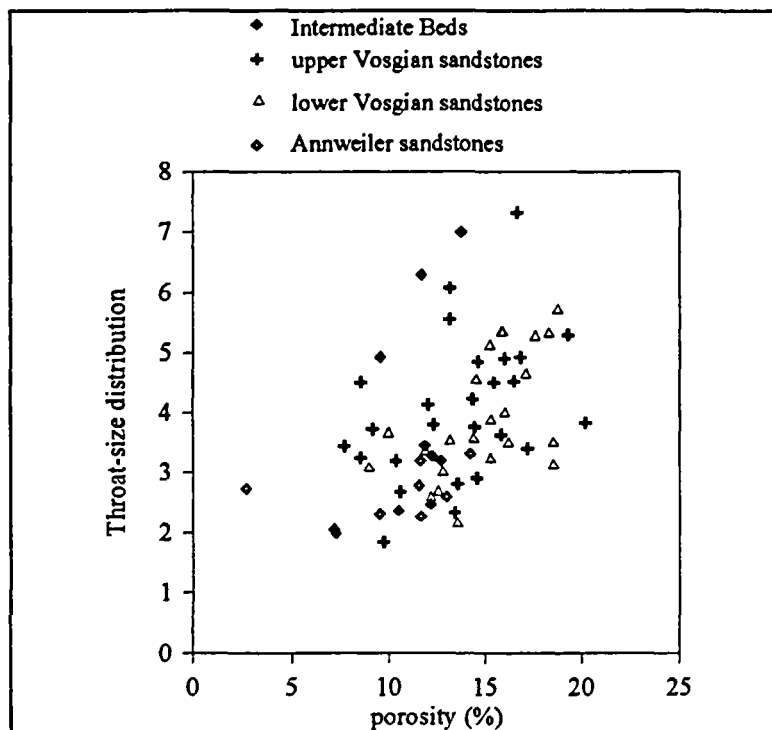


Fig. 18 - Plot of pore-throat-size distribution (PTD) vs. porosity for the four main Buntsandstein level.

6.2. PERMEABILITY

The permeability values were derived from nitrogen flow measurements by applying Forshheimer equation for gases (Noman and Kalam, 1991). They vary between less than 0.001 mD and 285 mD (Fig. 19). The highest permeabilities are concentrated in a zone of about 40 m thickness between 1120 and 1160 m depth in the upper Vosgian sandstones. The Intermediate Beds shows permeability values lower than 2 mD except for one sample. The lower Vosgian sandstones also have low permeability values (< 10 mD) except between 1216 and 1250 m where it varies between 10 and 100 mD. Finally, the base of the Buntsandstein sandstones (Annweiler sandstones and base of lower Vosgian sandstones) exhibits the poorest permeability values (< 1 mD).

The study of correlation between permeability and total porosity is classic for the evaluation of reservoir properties, even if it is now admitted that the porosity value is not a good indicator of transport properties for crustal rocks because of their inhomogeneous character. In EPS-1 sandstones, the variation of permeability can be very important even on a few centimetres scale. For example at 1158 m depth the permeability varies from 2 to 285 mD in 10 cm. Figure 19 confirms the low correlation between porosity and permeability and the fact that sandstones can have similar porosity but marked different permeability. In the case of Soultz Buntsandstein sandstones, samples with about 15% of porosity have permeability which can vary by more than three orders of magnitude.

The macro-porosity is more representative of the larger pathways which condition the permeability ; in the case of EPS-1 sandstones, the two parameters are well correlated with (Fig. 20). For Swanson (1981), at the lower saturations, the corresponding mercury pressure is not representative of pore sizes controlling bulk flow and applies only to the connection of the large-scale tortuous paths. This author considers it is necessary to reach a higher pressure which corresponds to pore size effectively interconnecting the total major pore system and thus, those that dominate fluid flow. This pressure corresponds to the maximum of S_{Hg}/P_c . The correlation between $(S_{Hg}/P_c)_A$ and permeability is very similar to the one between permeability and macro-porosity. In fact $(S_{Hg}/P_c)_A$ and macro-porosity are more or less equivalent parameters (Fig. 21).

The respective influence of macro-porosity and micro-porosity on permeability was tested from a permeability simulation model based on conducting network theory (Ochi, 1994). The permeability was computed from the mercury throat size distributions for 4 core samples. In a first step the permeability K_1 is computed from the whole distribution, then a permeability K_2 is computed from the distribution only relative to the micro-porosity. Table 5, where K_m is the experimental permeability, shows that the micro-porosity influences less than 25% of permeability even when it represents more than 85% of total porosity. At the opposite when micro-porosity is lower than macro-porosity, its effect on permeability is neglectable. For a ratio between micro-porosity and total porosity of about 0.8 (which is the mean ratio for the 67 Buntsandstein samples), the micro-porosity influences less than 10% of permeability. These results confirm the prevailing influence of macro-porosity on transport properties especially in the medium and high permeability range (> 10 mD).

	Φ_t (%)	Φ_m (%)	Φ_m/Φ	K_1 (mD)	K_2 (mD)	K_2/K_1	K_m (mD)
1214a	13.15	10.7	0.814	69	6	0.087	40
1221b	16.8	6.06	0.361	352	4.3	0.01	285
1745b	15.3	13.4	0.876	2.3	0.54	0.23	0.55
947b	10.6	9.4	0.887	1.9	0.35	0.18	1.25

Table 5. Influence of macro-porosity on permeability

The large variations of permeability in the Soultz Buntsandstein sandstones are strongly related to the heterogeneity of pore space which can be explained by the different conditions of sedimentation and pore geometry modification during diagenetic evolution. An other possible reason is the influence of clays on pore space and fluid flow properties, especially when they are dispersed (Neasham, 1977, Pittman and Thomas, 1979). The petrographic and diagenetic study put in evidence the existence of clay minerals (illite and mixed-layer clays). The clay content was not estimated from thin section but a shaliness index was derived from the gamma-ray log. This index is not equal to the clay content in absolute value. It only gives an estimation of clay content variation. The correlation between permeability and shaliness index is not significant even for Vosgian sandstones (Fig. 22). The shaliness index values for Intermediate Beds are not representative because of the presence of organic matter which has a strong influence on gamma-ray measurements.

Clay minerals and more generally fines, have an influence on formation damage and well productivity (Krueger, 1986) and a few percent of fines can damage a reservoir. This aspect is of major importance for geothermal exploitation where large amounts of brine are injected at high flow rate. The permeability decline by fines migration and blocking was put in evidence with flow tests (Ochi et al., 1993; Priisholm et al., 1987) and emphasises the importance of fines study (every matrix-filling minerals and not only clays) for estimation of reservoir properties.

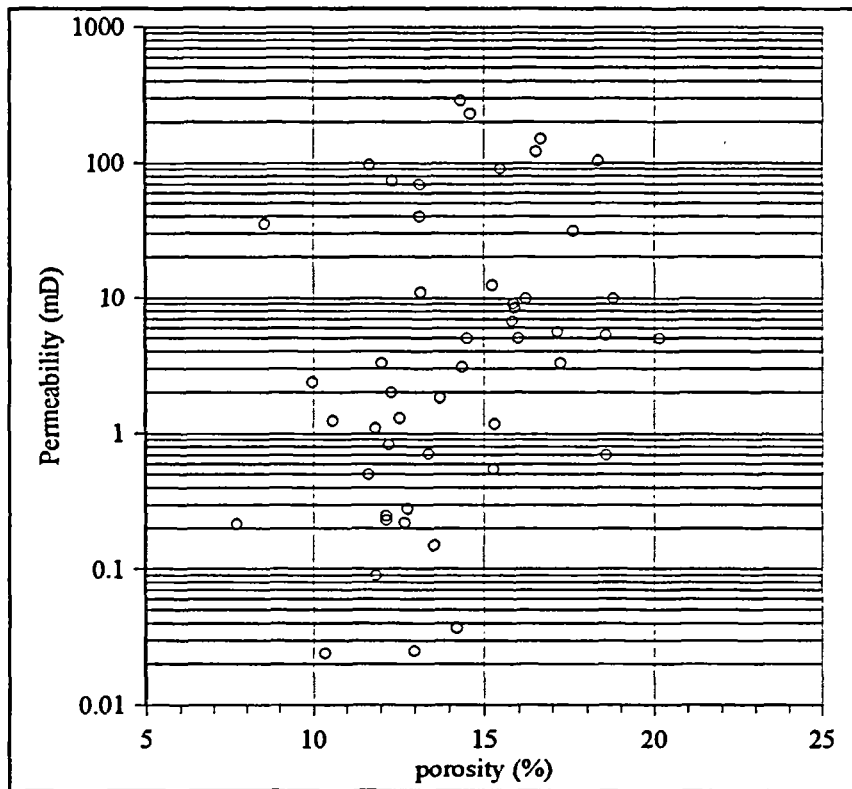


Fig. 19 - Semi-log plot of permeability vs. porosity.

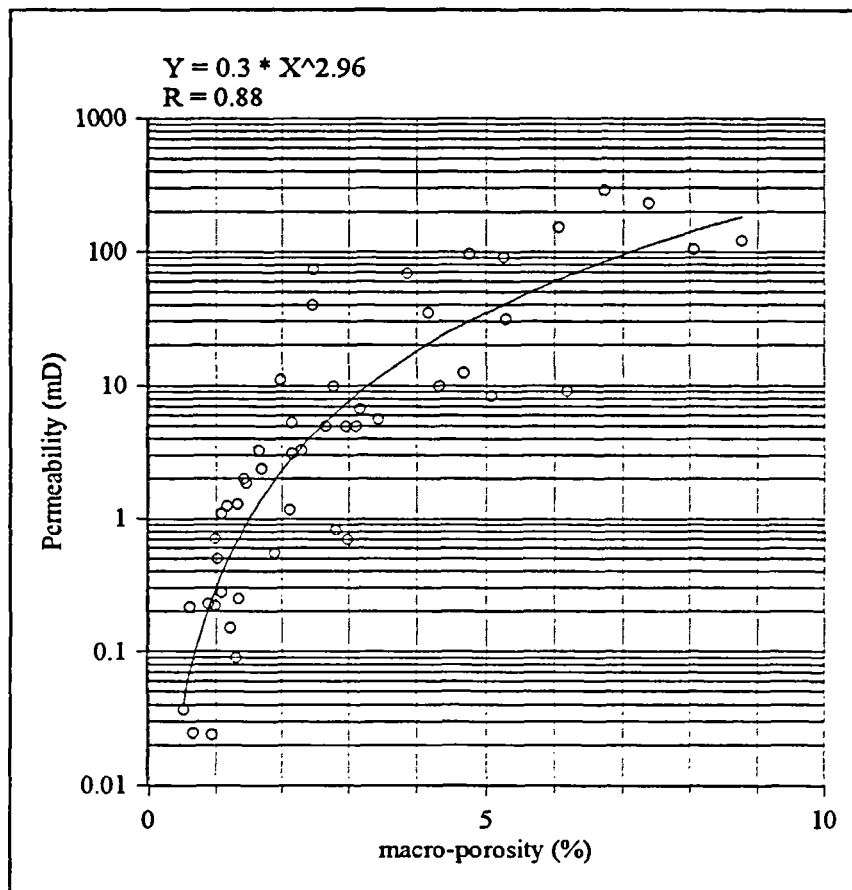


Fig. 20 - Semi-log plot of permeability vs. macro-porosity

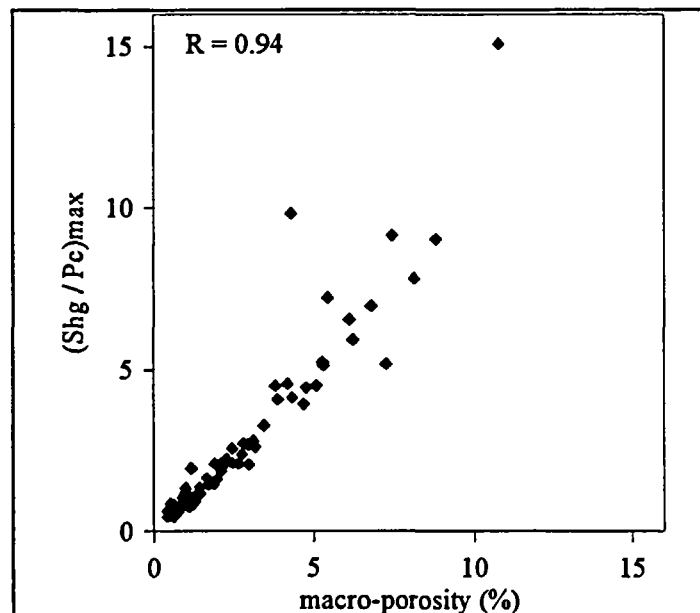


Fig. 21 - Plot of macro-porosity vs. $(S_{Hg} / P_c)_{max}$.

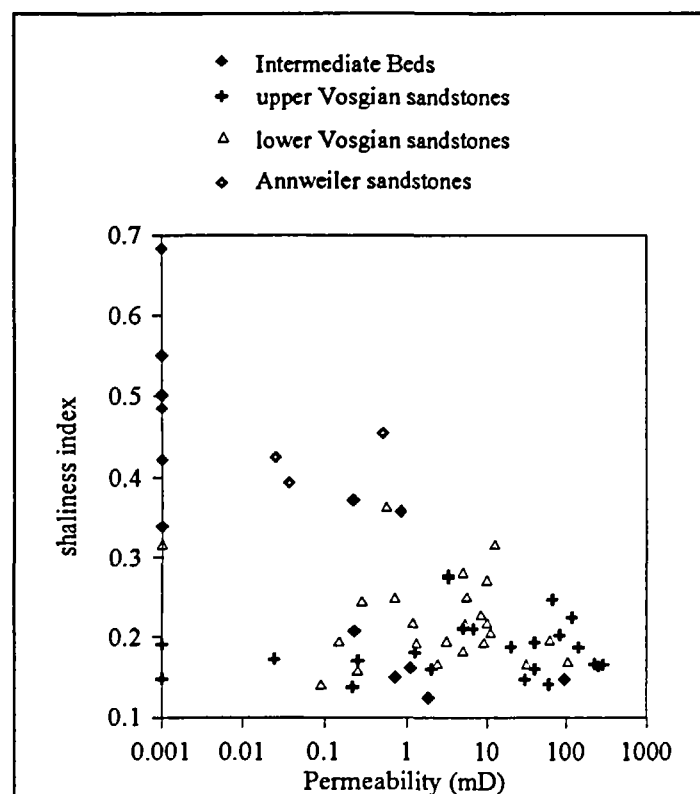


Fig. 22 - Semi-log plot of shaliness index vs. permeability for the four main Buntsandstein units.

7. RESERVOIR QUALITY EVOLUTION

7.1. LITHOLOGICAL SUB-UNITS OF LOWER TRIASSIC SANDSTONES

The combination of petrophysical data with well logging data (gamma ray, core gamma density measurements, sonic velocity) was used for characterising the different potential types of sandstones reservoirs. Their petrophysical behaviour was analysed according to the different geological sub-units of the lower Triassic formation providing regional guidelines for estimating their geothermal potential.

The sedimentary cover composed of Permian and lower Triassic formation (Buntsandstein) overlies the granitic basement. Gamma ray curve which recorded the natural radioactivity intensity was useful for characterising the three main lithological sub-units of Buntsandstein (Figures 2 and 23).

- the lower part (1350 - 1418 m) corresponding to Permian sandstones and lower Buntsandstein (Annweiler sandstones) are clay-rich sub-unit inducing a high gamma ray response.
- the intermediate part (1085 - 1350 m) corresponding to middle Buntsandstein is composed of red sandstones (Vosgian sandstones) and is characterised by steady and rather low gamma ray values.
- the upper part (1008 - 1085 m) is an organic-rich unit which shows a high radioactive content. This unit corresponds to the upper Buntsandstein (Intermediate Beds).

The comparison between different types of porosity profiles (core gamma density measurements, sonic log, mercury porosity) versus depth is presented in Figure 23. These curves are similar whatever the method used for evaluating the porosity. Mercury porosity data are rather higher than both sonic porosity and gamma density porosity data. In the Annweiler sandstones formation, porosity values are lower (10%) and correspond to microporosity mainly. In the Vosgian sandstones formation, the average mercury porosity is 13%, the sonic porosity is 10% and the gamma density porosity is 7% but porosity curves are more irregular. The mercury porosity values range between 15 and 20% in the higher porous levels (1115 to 1145, 1220, 1330 m). These zones are characterised by a high macroporosity. When the hydrothermal sealing is significant (1175, 1200 m), gamma and sonic porosity data are very low. In the upper Buntsandstein, the average porosity value is 8% and 12% locally (1080 m). Macroporosity is negligible in this formation.

Porosity profiles are compared with natural fractures density observed on cores. High fracture density values (5 joints/meter) correspond to low porosity values. Where fractures are lacking, both the highest porosity values and gas permeability data are measured (1115 - 1145 m). The correlation between macroporosity and permeability is clear. Hydrothermal filling sealed the fractures themselves and their surrounding inducing a strong decreasing of matrix porosity around the fractured zones.

7.2. RESERVOIR QUALITY EVOLUTION THROUGH DIAGENESIS

Potentially good reservoirs, as defined by their depositional environment, were located in Vosgian sandstones. Then a set of diagenetic phases influenced the quality of these initial reservoirs:

1. Early pedogenetic transformations slightly reduced the initial reservoir quality of Vosgian sandstones and Annweiler sandstones.
2. Early burial diagenesis induced a general decrease in intergranular porosity, by grain rearrangement and early silicification, but those early modification maintained the initial distribution of reservoirs.
3. Clay authigenesis led to a general decrease of intergranular porosity: Primary intragranular pores of 200 to 300 μm are filled with lattice-shape particles, leaving a residual microporosity
4. Silicification decreased porosity of coarse grained sandstone beds.

Geological and petrophysical parameters of a deep fractured sandstone formation

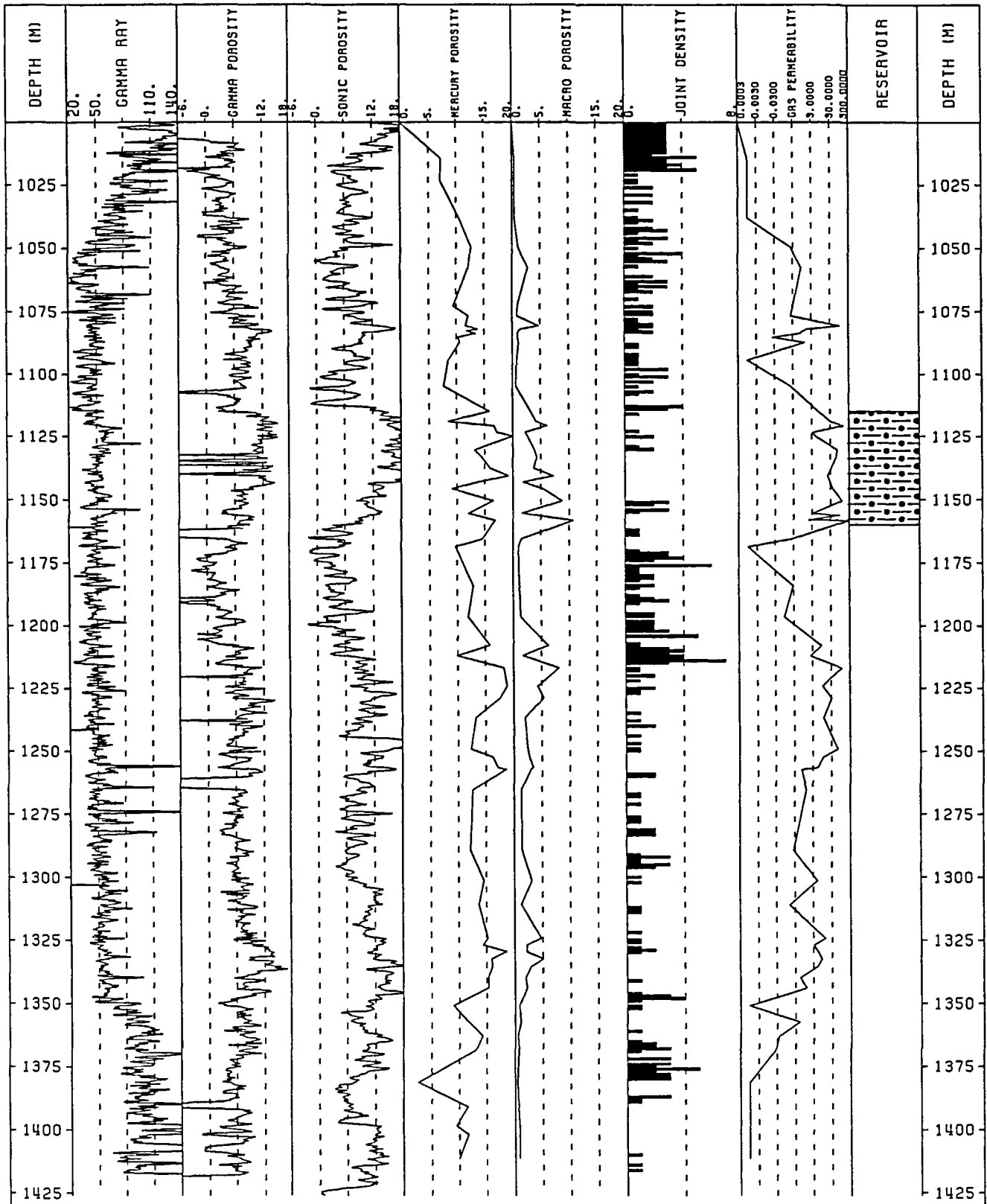


Fig. 23 - Synthetic composite log of Lower Triassic sandstones (Buntsandstein) from core analysis in the EPS-1 well (Alsace, France). Formation names are given according to M nillet et al. (1989). Gamma Ray curve gives the natural radioactivity, gamma porosity is deduced from continuous gamma-density measurements performed on core sections, sonic porosity is deduced from well logging data, mercury porosity is measured on selected samples, joint density is recorded from core analysis and gas permeability is performed on selected samples.

5. Even if feldspar alteration increased the intragranular porosity of fine grained beds, its influence is not significant on permeability.
6. Mineralisations linked with fracturation in the wall rock modified the distribution of reservoirs. The first silicification phase led to a decrease of intergranular porosity, in coarse and clean sandstone beds. Its main effect was to build an impervious barrier that would have preserve the underlying Lower Vosgian sandstone from further circulation. Later tectonic events reopened the fractures and favoured the circulation of barite-rich fluids.
7. Circulation of a barite-rich fluid essentially in the upper part of Vosgian sandstone progressively decreased fracture porosity and coarse grained sandstone beds porosity.
8. Dissolution of barite slightly increased the matrix porosity.
9. Circulation of fluids with organic matter, essentially in the upper part of Vosgian sandstone, progressively decreased fracture porosity and coarse grained sandstone beds porosity.

As a conclusion, the set of diagenetic phases induced a plugging of both porous matrix and fractures zones and strongly decreased the quality of the initial reservoirs.

7.3. CURRENT RESERVOIR QUALITY

The combination of petrophysical data (porosity, gas permeability) with geological data (natural fractures distribution) is helpful for characterising present day sub-units of Buntsandstein showing common petrophysical behaviour. These sub-units are reported on Fig. 24.

The best current reservoirs correspond to poorly fractured zones with both relatively high porosity (between 10 and 20%) and permeability (up to 300 mD). They are located within Vosgian sandstones sub-units (1125 - 1160 m, 1220 - 1250 m). Locally, porous levels with oil impregnation in matrix porosity occur (1115 - 1125 m) as well as stratified multilayer levels which are characterised by horizontal porous levels with oil impregnation in matrix porosity intercalated between tight levels (upper part of Vosgian sandstones: 1102 - 1103 m; 1107 - 1110 m) .

The upper part of the Buntsandstein (1009 - 1020 m) and the middle part of Vosgian sandstones (1178 - 1215 m) are highly naturally fractured sandstones affected by hydrothermal circulation which have fully sealed the matrix porosity. These levels show high secondary cementation associated with fracturation and have a bad reservoir quality.

The remaining levels represent poorly fractured zones with a low matrix porosity and permeability. These levels correspond to Permian formation, Annweiler sandstones and several parts of middle and upper Buntsandstein (VOLTZIA sandstones for example) and have a very bad reservoir quality.

Finally it is clear that the current reservoir quality of Buntsandstein formations along the EPS-1 well is weak. For most of the geothermal exploitations in sandstones, the permeability measurements on cores give values greater than 300 mD. And here the fracturation does not seem to enhance the reservoir quality. But we must keep in mind that these conclusions result from the study of a single well and cannot be easily extrapolated to the whole zone of the Soultz geothermal anomaly.

Geological and petrophysical parameters of a deep fractured sandstone formation

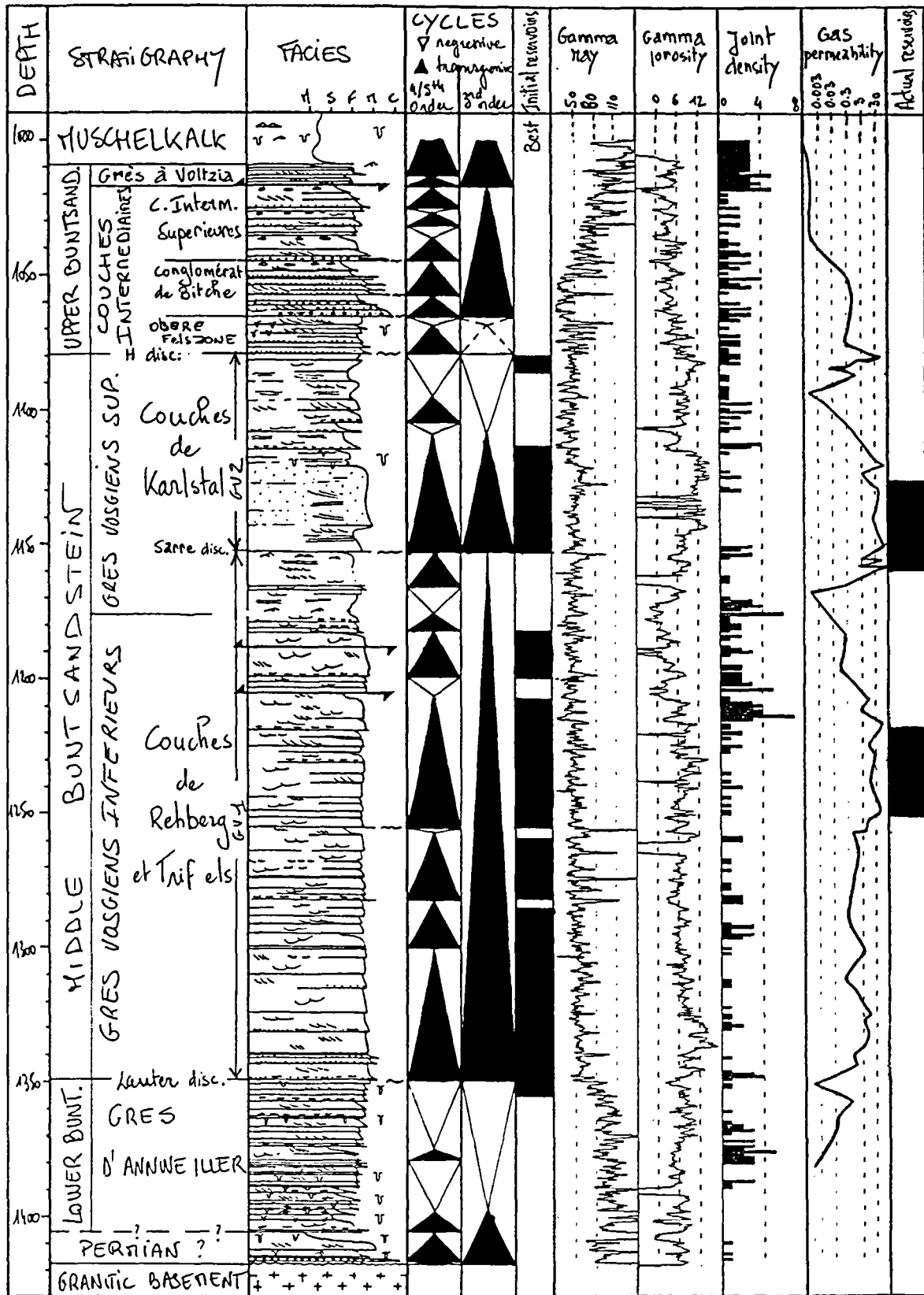


Fig. 24 - Sedimentological log of EPS1 borehole. Location of initial and current best reservoir units.

CONCLUSION

The sedimentological analysis (lithology, facies sequences, discontinuities, depositional environment) of the EPS1 silicoclastic succession enabled a qualitative evaluation of the initial properties of the stratigraphic units before the diagenetic and tectonic changes that have been responsible for the present reservoir qualities.

The deposits, intersected by Borehole EPS1, are continental and predominantly arenaceous, and regionally comprise four major formations: (i) the Annweiler sandstone (basal unit), (ii) the Vosgian sandstone (lower middle unit), (iii) the Intermediated Beds (upper middle unit), and, (iv) the Voltzia sandstone (upper unit). From a sedimentological analysis, a set of the best initial reservoirs was defined qualitatively. Owing to the presence of numerous shale intervals and thinness of the sandy beds, the initial reservoir quality of the Annweiler formation was relatively mediocre. The best initial reservoirs in the Vosgian sandstone were parts of the sedimentary sequence where an important vertical aggradation combined with a strong hydrodynamic regime favoured the deposition of thick sandstone bodies with little clays. The initial reservoir quality of the Intermediate Beds was poorer than that of the Vosgian sandstone. This is due to facies heterogeneity, numerous sedimentary discontinuities, thinness of the sequences and early dolomitization. Because of the thinness of the sequences and the presence of numerous shale interbeds, the Voltzia sandstone was a good initial reservoir. Therefore, the best initial reservoirs were mainly located in the thickest unit of the Buntsandstein, namely the Vosgian sandstones.

An evaluation of diagenetic phases was carried out from thin sections analysis. The Triassic sediments of the well EPS1 underwent diagenetic events characterized by mineral precipitation and dissolution in cement and fractures and by replacement of primary minerals. A comparison of the successive diagenetic events enabled to understand the role of precipitation and/or dissolution processes in the reservoir quality evolution. The petrographical study showed that early diagenetic processes (pedogenetic phases, feldspar alteration) did not affect significantly the initial porosity of these sediments. On the other hand other diagenetic events (clay minerals, barite, quartz) induced mineral deposition decreasing the porosity. The silicification phase in the Vosgian sandstone, linked with fracturing, considerably decreased the intergranular porosity of coarse grained sandstone bed at the fracture walls and created on a short distance an impervious barrier close to the fracture. This impervious zone was able to preserve the underlying reservoir from later fluid circulations and related deposition and to maintain its initial porosity.

Fracture density (0.85 fracture per meter), which is rather high in this clastic formation, clustering organization of fractures, and their dominant nearly-meridian striking azimuth (Rhenan direction) suggested that the fractures properties were predominantly governed by the Rhine graben tectonic activity. Therefore, the occurrence of these fractures generated by an extensional regime would be favourable for fluid circulations. The structural evaluation of cores has confirmed the role of the fractures in the paleofluid circulations. The cluster organization of fractures associated to their significant mineral filling show that fractures act nowadays as impervious barrier. The natural fractures were good pathways for fluid circulations but now the current fracture network seems to be completely sealed in this well.

The clastic dikes, which are mainly sealed by early lithic sediments (sandstone), do not induce a strong anisotropy within the Buntsandstein. They constitute minor heterogeneity and do not really influence the reservoir properties in terms of permeability. Occurrences of organic compounds in fracture planes suggest migrations from the closest Pechelbronn oil fields through the fracture network.

The main fault is located at 1200 m depth, and its surrounding was affected by the precipitation of silica and barite. This wall rock effect is visible from about 1 or 2 m thick. Now, this fault acts as a impervious barrier and represents a tight limit between two major blocks within the Buntsandstein formation. Then, fault sealing reduces the reservoir quality within the cementation zone which is roughly developed parallel to the fault.

From an exhaustive petrophysical database, the relationship between porosity and permeability were investigated. Even though the average porosity of the Buntsandstein is rather high (12%), the permeability is

rather low suggesting that connected porosity is partly plugged by mineral precipitation related to diagenetic processes. The heterogeneity of permeability in the Soultz Buntsandstein sandstones is strongly related to the heterogeneity of pore space which can be itself linked to the different conditions of sedimentation, the modifications of pore geometry during diagenetic evolution and the occurrences of clay minerals in the porous matrix.

Surprisingly, no evidence of natural water outflow was detected in EPS-1 well, even within highly fractured zones. However, in the same Buntsandstein unit, 4550 and GPK-1 wells, located at a short distance of EPS-1, revealed outflows of hot water or fluid losses during the drilling through the major fault zones. From an hydraulic point of view, the natural behaviour of a given major fault is therefore strongly heterogeneous.

In the EPS-1 well, the Vosgian sandstone between 1115 and 1160 m, is the best potential reservoir with formation temperature ranging between 120 and 125 °C and permeability of about 100 mD. The lower part of this zone is spatially limited by a highly fractured and hydrothermally sealed zones (1168 - 1215 m). Natural fracture zones act as permeability barrier within these deep sandstones. Field work carried out on Permo-Triassic sandstones in Great Britain (Knott, 1994), indicated that the width of a fault zone increases as fault displacement and consequently reduced the permeability of the deformed reservoir by sealing.

REFERENCES

- AIGNER T., BACHMANN G.H. (1992) - Sequence stratigraphy framework of the German Triassic. *Sedimentary Geology*, 80, pp. 115-135.
- ALBERTI F. (1834) - Beitrag zu einer Monographie des Bunten Sandsteins, Muschelkalks und Keupers, und die Verbindung dieser Gebilde zu einer Formation. Cotta Stuttgart-Tübingen, 366 p.
- BERGERAT F. (1985) - Déformations cassantes et champs de contraintes tertiaires dans la plate-forme européenne, Ph.D. Thesis, 317 pp., Univ. Pierre et Marie Curie, Paris VI.
- BENDERITTER Y., TABBAGH A., ELSASS P. (1995) - Calcul de l'effet thermique d'une remontée hydrothermale dans un socle fracturé, Application à l'anomalie géothermique de Soultz-sous-Forêts (Nord Alsace), *Bull. Soc. géol. France*, 166, 37-48.
- BERGERAT F. (1987) - Paléo-champs de contraintes tertiaires dans la plate-forme européenne au front de l'orogène alpin, *Bull. Soc. Geol. Fr.*, III, 3, 611-620.
- CASSAGNABERE A. (1993) - Rôle des modifications texturales et géochimiques des argiles dans la baisse de perméabilité d'un grès argileux soumis à la circulation d'une saumure. DEA Matériaux Minéraux, BRGM, LPAH, Univ. d'Orléans, 49 p.
- CHILES J.P., COURRIOUX G., DEVERLY F., RENARD P. (1993) - 3D Geometric modelling of layers and fault system using Gocad software: the example of the horst of Soultz (Alsace, France), *Geoinformatics*, 4, 3, p. 209-218.
- DACHROTH W. (1985) - Fluvial Sedimentary Styles and Associated Depositional environments in the Buntsandstein West of River Rhine in Saar Area and Pfalz (F.R. Germany) and Vosges (France). In Mader D. (Editor). *Aspects of fluvial sedimentation in the lower triassic Buntsandstein of Europe. Lectures Notes in Earth Sciences*, 4, p.197-248, Springer ed.
- DUBOIS M., AYT OUGOUGDAL M., ROYER J.J., CATHELINÉAU M. (in press) - Paleo and actual geothermal circulations in the Soultz-sous-Forêts granite (Rhine Graben, France).
- DUMAS and BELPAUME (1991) - Résultats préliminaires des mesures non destructives de gamma densimétrie sur des carottes de grès triasique de Soultz-sous-Forêts. BRGM internal report 91 NT 096 SGN/IMRG, 21 p., 10 appendices.
- FLORES E.L., ROYER J.J. (1992) - Convective heat transfer around the Soultz-sous-Forêts geothermal site (Rhine Graben). In: BRGM Eds doc. 223, VIth Int. Symposium Continental Scientific Drilling Programs, Paris.
- FRIEDENBERG R. (1994) - Stratigraphie génétique des dépôts continentaux du Buntsandstein de l'Est du bassin de Paris. Application aux stockages de gaz naturel en nappe aquifère. Extension au bassin de Paris. Thèse de l'Université Louis Pasteur de Strasbourg.
- GENTER A., TRAINÉAU H., DEZAYES C., ELSASS P., LEDESERT B., MEUNIER A., VILLEMINE T. (1995).- Fracture analysis and reservoir characterization of the granitic basement in the HDR Soultz project (France). *Geotherm. Sci. & Tech.* Vol. 4 (3), p. 189-214.

GENTER A., TRAINÉAU H. (1993) - Fracture distribution from core analyses in the basement of the Rhine graben, in Proc. European Union of Geosciences, EUG VII 4-8 April 1993, Strasbourg, Terra Nova, 5, Abstract, 1, p. 217-218.

GENTER A., TRAINÉAU H. (1992) - Borehole EPS-1, Alsace, France: preliminary geological results from granite core analyses for Hot Dry Rock research, Sci. Drilling, 3, 205-214.

HOUSSE B.A. (1984) - Reconnaissance du potentiel géothermique du Buntsandstein à Strasbourg - Cronenbourg. Géothermie Actualités, n°1, p. 36-41.

JONES S.C. (1987) - Using the inertial coefficient, β , to characterize heterogeneity in reservoir rocks. SPE 16949. 62th Annual technical Conference and Exhibition of the Society of Petroleum Engineers held in Dallas, p. 165-174.

KNOTT S.D. (1994) - Fault zone thickness versus displacement in the Permo-Triassic sandstones of NW England, J. Geol. Soc., London, 151, p. 17-25.

KRUEGER R.F. (1986) - An overview of formation damage and well productivity in oilfield operations. J. Petroleum Technology, p. 131-152.

LECARLIER, C., J.J. ROYER, FLORES E.L. (1994) - Convective heat transfert at Soultz-sous-Forêts geothermal site. Implications for oil potential, First Break, 12, p. 553-560.

LEPPLA A. (1988) - Über den Buntsandstein im Haardtgebirge (Nordvogesen). Geognostische Jahreshefte, Band 1, Kassel.

MAGET P., WALGENWITZ F., TIETZE R. (1979) - Synthèse géothermique du fossé rhénan supérieur, Rapport CCE-DGRST.

Mc PHEE C.A., ARTHUR K.G. (1991) - Klinkenberg permeability measurements: problems and practical solutions, In Advances in core evaluation II: Reservoir appraisal, edited by P.F. Worthington, p. 371-391.

MARSILY G. de (1993) - Quelques méthodes d'approche de la variabilité spatiale des réservoirs souterrains, Hydrogéologie, n° 4, p. 293-302.

MELAS F.F., FRIEDMAN G.M. (1992) - Petrophysical Characteristics of the Jurassic Smackover Formation, Jay field, Conecuh Embayment, Alabama and Florida: AAPG Bulletin, v. 76, n° 1, p. 81-100.

MENILLET F., COULOMBEAU C., GEISSERT F., KONRAD H.J., SCHWOERER P. (1989) - Geological map of France, sheet Lembach, 168, scale 1/50000, edited by BRGM, Orléans.

MENJOZ, A., J.P. CAUTRU, A. CRIAUD, A. GENTER (1988) - Stimulation des réservoirs géothermiques en milieu cristallin, BRGM IMRG Annual Open File Rep., p. 35-42.

MORAES M.A.S. (1991) - Diagenesis and Microscopic heterogeneity of lacustrine deltaic and turbidic sandstone reservoirs (Lower Cretaceous), Potiguar Basin, Brazil. AAPG Bulletin, v. 75, n° 11, p. 1758-1771.

NEASHAM J.W. (1977) - The morphology of dispersed clay in sandstone reservoir and its effect on sandstone shaliness, pore space and fluid properties. SPE 6858, 52th annual tech. conf. and exh. of the SPE of AIME, Denver, CO, Oct. 9-12.

NOMAN R., KALAM M.Z. (1991) - Transition from laminar to non-Darcy flow of gases in porous media. In *Advances in core evaluation: Accuracy and precision in reserves estimation*, edited by P.F. Worthington, p. 447-462.

OCHI J. (1994) - Etude et modélisation de la chute de perméabilité en relation avec l'injection de fluides dans les réservoirs argilo-gréseux. Thèse de doctorat, Université Paris XI, Orsay.

OCHI J., VERNOUX J.F., FOUCHER J.C., GENTER A. (1993) - Experimental percolation in argillaceous sandstones and survey of permeability and porosity changes: Application to the reinjection of cooled brines into geothermal reservoirs, *Geofluids' 93 Int. Conference*, Torquay, p. 223-227.

PITTMAN E.D, THOMAS J.B. (1979) - Some applications of scanning electron microscopy to the study of reservoirs rocks. *J. Pet. Tech.*, p. 1375-1380.

PRIISHOLM S., NIELSEN B.L., HASLUND O. (1987) - Fines migration, blocking and clay swelling of potential geothermal sandstone reservoirs, Denmark. *SPE Formation Evaluation*, p. 168-178.

RENARD P., COURRIOUX G. (1994) - Three dimensional geometric modeling of a faulted domain: the Soultz Horst example (Alsace, France), *Computers & Geosciences*, Vol 20, No. 9, p. 1379-139.

RICHTER-BERNBURG G. (1974) - Stratigraphische Synopsis des deutschen Buntsandstein. *Geol. jb. Dtsch.*, 25, p.127-132.

SCHELLSCHMIDT R., SCHULZ R. (1991) - Hydrothermic studies in the Hot Dry Rock project at Soultz-sous-Forêts. *Geotherm. Sci. Tech.*, 3, p. 217-238.

SCHLUMBERGER (1987) - Log Interpretation Principles/Applications, Porosity Logs, Chap.5, Schlumberger Educational Services, 32-55.

SCHNAEBELE R. (1948) - Monographie géologique du champ pétrolifère de Pêchebron, *Mém. Serv. géol. Als. Lorr.*, 7, 254 pp., Strasbourg.

SCHNEIDER C. (1984) - Les granitoïdes de la partie Nord-Est des Vosges moldanubiennes : évolution magmatique et structurale, Ph.D. Thesis, 202 pp., Univ. Louis Pasteur, Strasbourg.

SIZUN J.P., JEANETTE D. (1995) - Transformations pétrographiques successives conduisant à la structuration des réservoirs du Buntsandstein : le forage géothermique de Soultz-sous-Forêts (Alsace, France), *C.R. Acad. Sci. Paris*, t. 320, série II a, p. 365-372.

SWANSON B.F. (1981) - A simple correlation between permeabilities and mercury capillary pressures. *J. Petroleum Technology*, p. 2498-2504.

TENZER H., BUDEUS P., SCHELLSCHMIDT R. (1992) - Fracture analyses in Hot Dry Rock drillholes at Soultz and Urach by borehole televiewer measurements. *Trans. Geotherm. Res. Council*, 16, p. 317-321.

TERZAGHI R. (1965) - Sources of error in joint surveys. *Geotechnique*, 15, p. 287-304.

VAVRA C.L., KALDI J.G., SNEIDER R.M. (1992) - Geological application of capillary pressure: A review. *AAPG Bulletin*, v.76, n°6, p. 840-850.

VERNOUX J.F., BRACH M., FOUCHER J.C., MATRAY J.M., MENJOZ A., OCHI J., ROJAS J., DE LAS HERAS A. (1993). Etude expérimentale des problèmes de réinjection dans les grès: objectifs - méthodologie - protocoles. Rapport BRGM-Ademe SGN/IRG ARG 93 T13, 104p.

VERNOUX J.F., LAMBERT M. (1993) - Aquifères profonds d'Alsace: Constitution d'une base de données à usage géothermique. BRGM internal report ARG93T37, 41 p.

VILLEMEN T., BERGERAT F. (1987) - L'évolution structurale du Fossé Rhénan au cours du Cénozoïque : un bilan de la déformation et des effets thermiques de l'extension, Bull. Soc. Géol. France (8), t. III, n° 2, p. 245-255.

VILLEMEN T. (1986) - Tectonique en extension, fracturation et subsidence : le fossé rhénan et le bassin de Sarre-Nahe, Ph.D. Thesis, 270 pp., Univ. Pierre et Marie Curie, Paris.

VINCHON Ch., MATRAY J.M., ROJAS J. (1993) - Textural and mineralogical changes in argillaceous sandstones, induced by experimental fluid percolation: Geofluids' 93 Int. Conference, Torquay, England, p. 233-236.,

ZIEGLER P.A. (1982) - Geological Atlas of Western and Central Europe. Shell, The Hague, 130 pp.

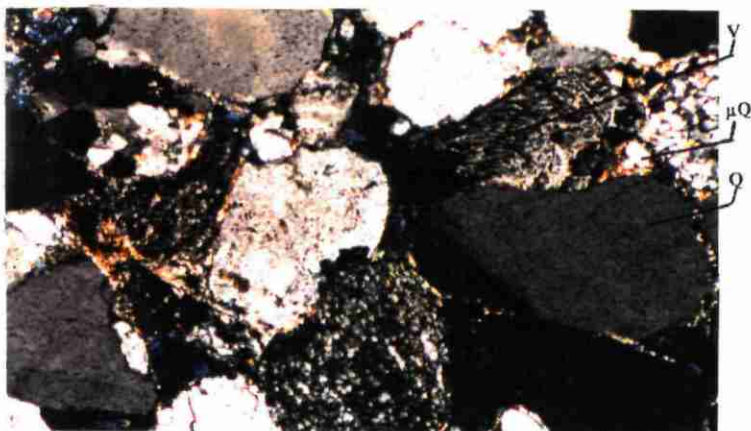
ZIEGLER P.A. (1992) - European cenozoic rift system. case history studies on rifts: european and asia, Tectonophysics, 208, p. 91-11.

Appendices

APPENDIX 1

PLATE 1

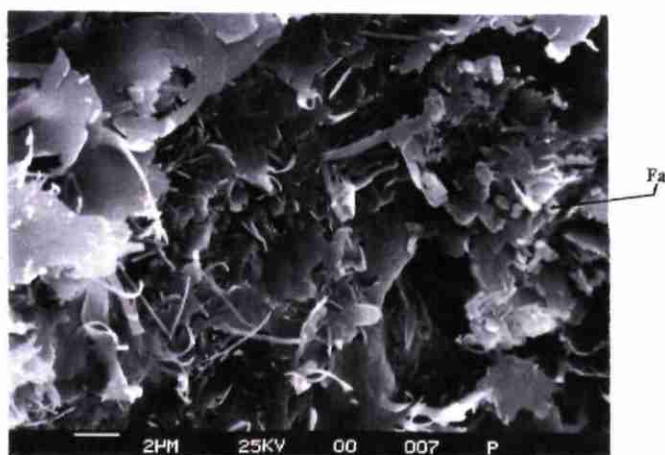
- Photo 1 1332.40 m. Lower Vosgian sandstone. Coarse detritic quartz (Q), Feldspar (F) and volcanic (V) and microquartzic (μ Q) lithoclasts . Clay coating of the detritic grains. Crossed nichols . 1 cm = 150 μ m
- Photo 2 1332.40 m. Lower Vosgian sandstone. Detail of a volcanic lithoclast : plagioclase needles in an amorphous matter. Iron oxydes. Crossed nichols, 1cm = 85 μ m
- Photo 3 1140.80 m Upper Vosgian sandstone: Illite lattices and plates coating the intergranular porosity. Right side of the photo, altered feldspar (Fa). Scanning electronic microscope, secondary electrons.
- Photo 4 1348.14 m Lower Vosgian sandstone. "Clastic dyke" : fracture with sandstone filling, from upper and coarse layers. Phenomena thought to be associated to early burial events.
- Photo 5 1359.01 m. Annweiler sandstone: Dolomite. Pedogenetic features.
- Photo 6 1365.29 m. Annweiler sandstone. Calcidolomitic nodules in clay matrix. Pedogenetic origin. 1cm = 570 μ m.



①



②



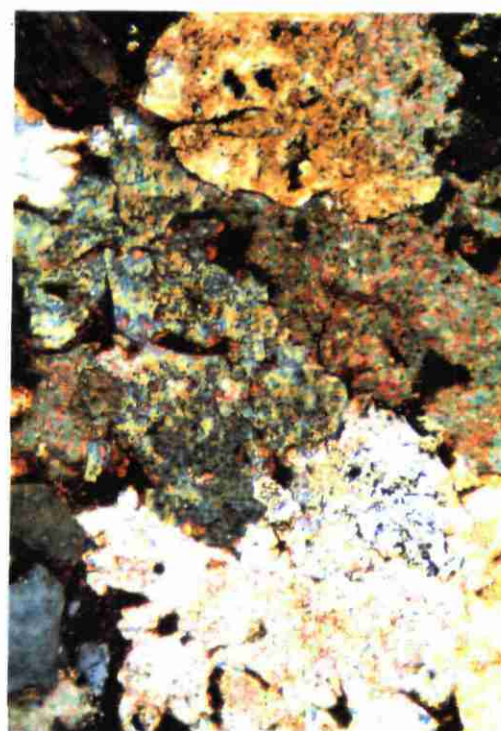
③



④



⑤



⑥

PLATE 2

- Photo 1 1332.40 m. Base of Lower Vosgian sandstone. Pedogenetic ankeritic cement (A), sparitised by early burial. Sideritic edging (S) likely to be synchronous of fracture filling siderite and linked to late tectonic diagenesis. Crossed nichols, 1cm = 570 μ m
- Photo 2 1158.05 m. Upper Vosgian sandstone. Pressure-dissolution features between grains (quartz/quartz, quartz/feldspar). Feldspar weathering with intragranular porosity. Uncrossed nichols, 1cm = 570 μ m
- Photo 3 1145.98 m. Upper Vosgian sandstone. Weathered feldspar, and clay filling (brown). Weathering likely to be prior to sedimentation, increased during burial, inducing a non-efficient intragranular porosity. Uncrossed nichols, 1cm = 570 μ m
- Photo 4 1158.25 m. Upper Vosgian sandstone. Illite-type clay, in more or less coalescent lattices, coating of early siliceous growth. Altered feldspar on the left of the photograph. Scanning electron microscope, secondary electrons.
- Photo 5 1204.0 m. Upper Vosgian sandstone. Fracture associated to the 1205m fault. Pink silicification of the wall rock. Reopening and barite fill.
- Photo 6 Wallrock of the former photo. Wallrock digestion : residual detritic quartz in a microquartzic matrix. Uncrossed nichols. 1cm = 150 μ m
- Photo 7 1145.98 m. Upper Vosgian sandstone. Authigenic quartz growth in clean sandstone. Small secondary quartz growth, associated to a late and dissolved baryte, 1cm = 570 μ m

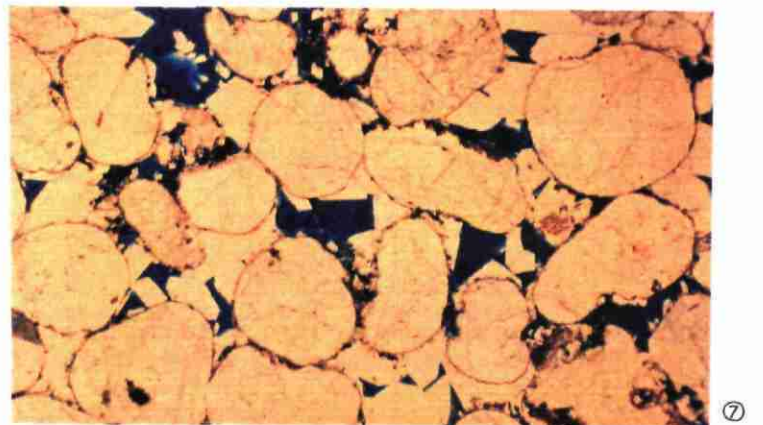
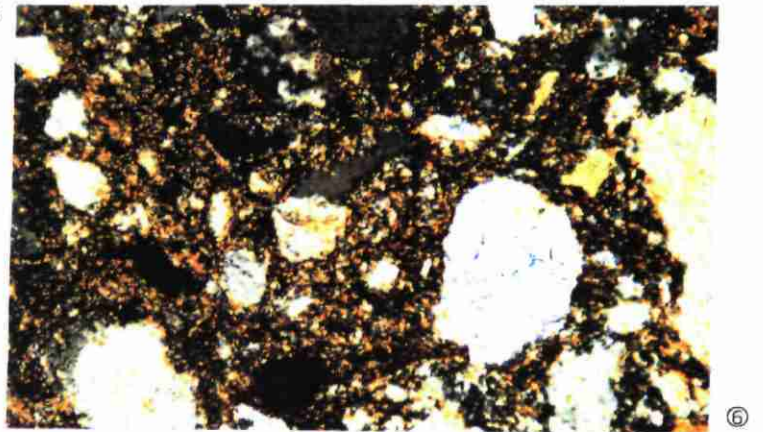
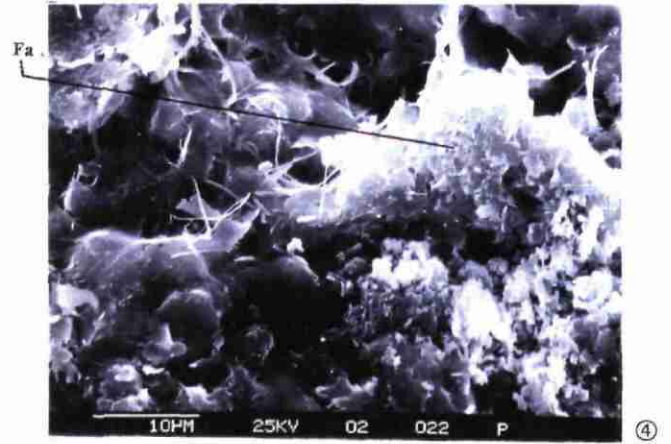
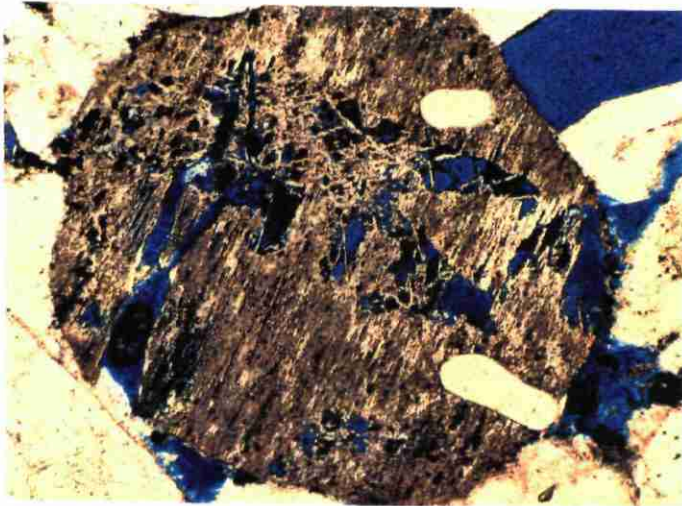
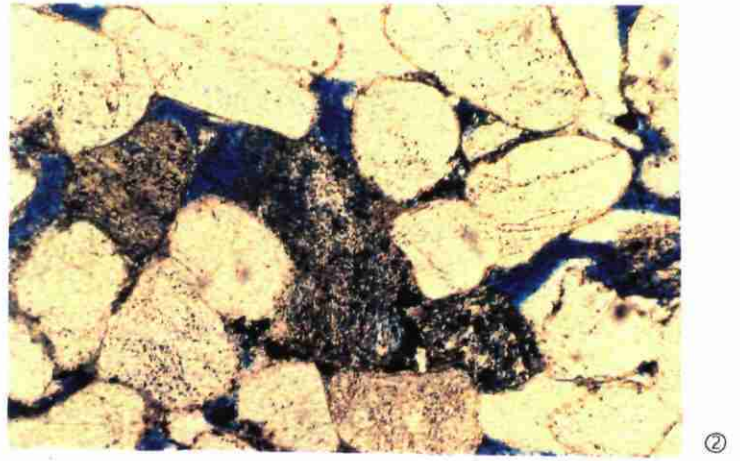
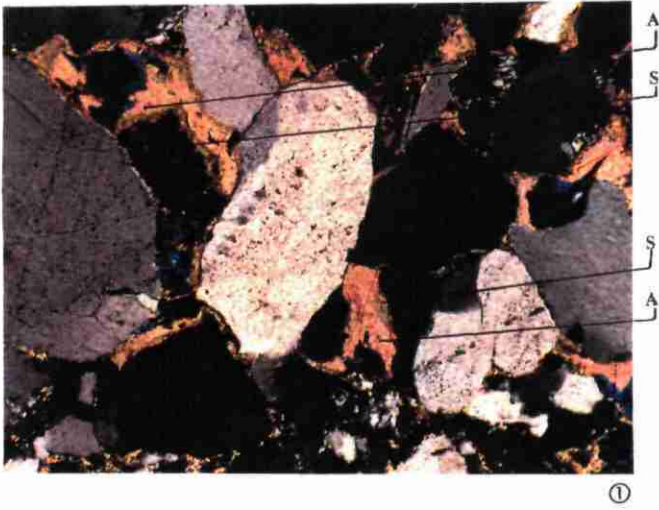
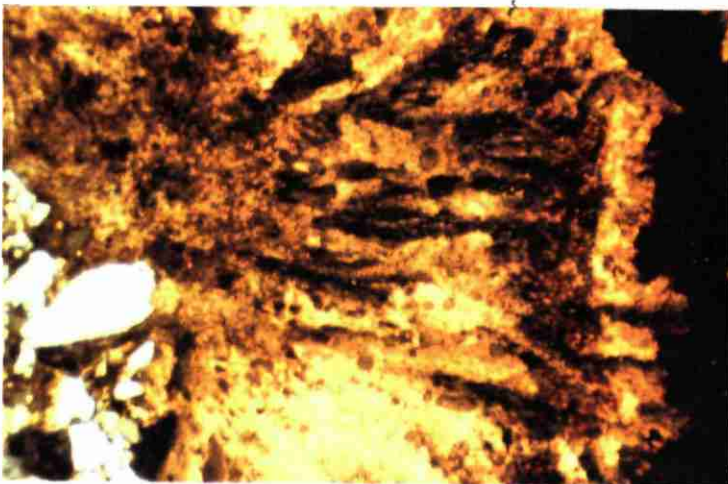


PLATE 3

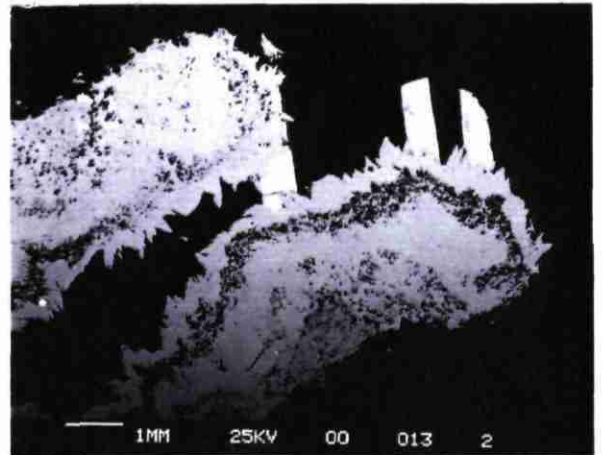
- Photo 1 1204m. **Upper Vosgian sandstone.** Plate 2 - Photo 5 fracture. Top of the photo : Silica-digested wall-rock, with residual detritic quartz grains. Towards center petaloide automorphic quartz, and late filling of barite. Crossed nichols, no blue filter. 1cm = 150 μ
- Photo 2 1097.52m. Top of **Upper Vosgian sandstone.** From left to right, from wall-rock to center of the filling, petaloid automorphic quartz, siderite, and organic matter. Crossed nichols, no blue filter. 1 cm = 150 μ
- Photo 3 1097.52m. Same as Photo 2 with scanning electronic microscope, back-scattered electron. Zonality of siderite is underlined, first automorphic, then collomorphic. Last phase automorphic.
- Photo 4 1214.32 m. **Lower Vosgian sandstone.** Bundle baryte in fractures, associated to small automorphic quartz. Crossed nichols, 1cm = 150 μ m
- Photo 5 1214.32 m. **Lower Vosgian sandstone.** Baryte (B) and quartz (Q), in cement. Crossed nichols 1cm = 570 μ m



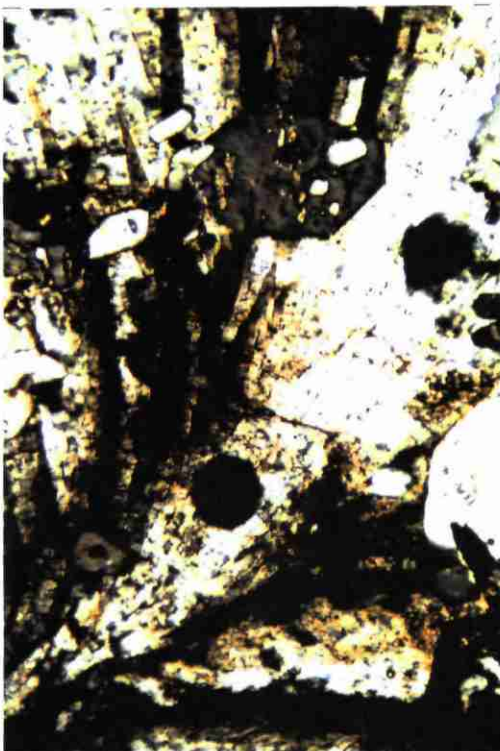
①



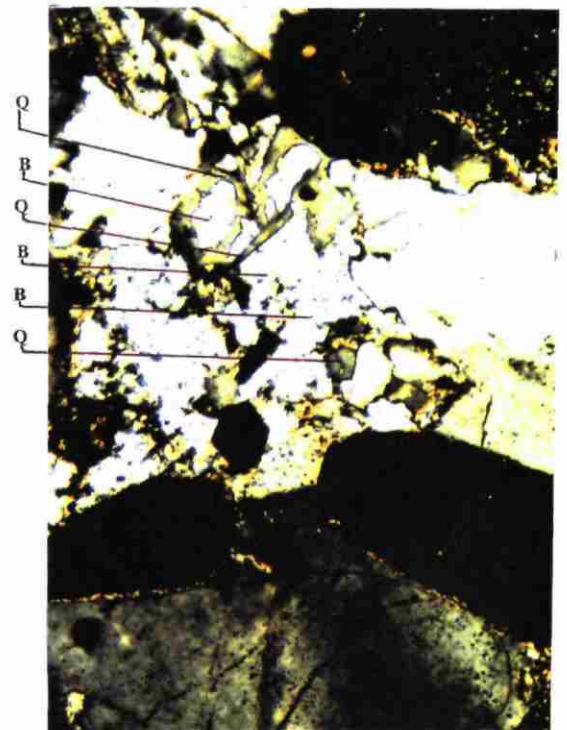
②



③



④



⑤

APPENDIX 2

Petrophysical data for the 67 cored samples of the EPS-1 borehole

1. core number
2. sample number
3. depth (m)
4. sonic porosity (%)
5. gamma-density (g/cm³)
6. gamma-porosity (%)
7. mercury-density (g/cm³)
8. mercury-porosity (%)
9. macro-porosity (%)
10. micro-porosity (%)
11. volume of injected mercury (mm³/g)
12. withdrawal efficiency (%)
13. withdrawal efficiency (mm³/g)
14. pore throat size distribution
15. maximum ratio S_{Hg} / P_c
16. shaliness index
17. permeability (mD)

Core #	Sample #	Depth m	sonic porosity %	gamma density g/cm3	gamma porosity %	Hg density g/cm3	Hg porosity %	macro porosity %	micro porosity %	Inj. Vol. mm3/g	We %	We mm3/g	PTD	Shg/Pc (max)	I sh	K mD
K013	706	1014.53	9.34	2.53	4.53	2.63	7.25	0.41	6.84	29.73	22	6.54	1.99	0.64	0.5	0.001
K015	738	1023.47	8.75	2.50	5.66	2.64	7.17	0.47	6.70	29.27	22	6.44	2.06	0.658	0.55	0.001
K017	792	1038.08	11.84	2.40	9.43	2.67	10.49	0.42	10.07	43.90	23	10.10	2.36	0.597	0.34	0.001
K018	830	1049.50	7.93	2.37	10.57	2.61	12.69	0.99	11.70	55.66	16	8.91	3.19	1.21	0.37	0.22
K021	855	1057.62	6.94	2.43	8.30	2.65	12.23	2.80	9.43	52.50	10	5.25	3.28	2.712	0.36	0.83
K023	896	1072.83	9.52	2.43	8.30	2.68	9.53	0.97	8.56	39.41	23	9.07	4.94	1.034	0.15	
K025	912	1076.71	6.80	2.34	11.70	2.60	12.16	0.88	11.28	53.38	21	11.21	2.47	1.023	0.21	0.23
K025	925	1080.78	13.22	2.37	10.57	2.62	11.68	4.76	6.92	50.60	13	6.58	6.29	4.437	0.15	97
K025	929	1081.99	16.62	2.33	12.08	2.63	13.74	1.46	12.28	60.53	31	18.76	7.00	1.2	0.12	1.85
K026	935	1082.78	14.18	2.31	12.83	2.56	11.85	1.08	10.77	52.47	20	10.49	3.44	0.981	0.16	1.1
K026	937	1083.68	9.87	2.33	12.08	2.61	13.40	0.98	12.42	59.33	28	16.61	2.32	1.337	0.15	0.71
K026	943	1085.28	9.85	2.42	8.68	2.61	10.35	0.93	9.42	44.24	26	11.50	3.19	1.113	0.17	0.024
K026	947	1087.25	9.00	2.36	10.94	2.60	10.58	1.16	9.42	45.41	30	13.62	2.68	1.945	0.18	1.25
K027	970	1094.27	10.46	2.43	8.30	2.63	8.52	0.77	7.75	35.39	35	12.39	3.24	0.607	0.19	0.001
K029	1004	1104.86	4.84	2.35	11.47	2.61	7.68	0.61	7.07	31.91	29	9.25	3.44	0.83	0.14	0.217
K031	1039	1114.93	13.78	2.28	13.96	2.60	15.82	3.16	12.66	72.27	28	20.24	3.62	2.607	0.21	6.7
K032	1057	1119.12	17.98	2.28	13.96	2.64	8.56	4.16	4.50	35.56	21	7.47	4.51	4.541	0.15	35
K032	1061	1120.88	15.85	2.20	16.98	2.62	16.66	6.06	10.60	76.45	23	17.58	7.32	6.558	0.19	152
K032	1072	1123.52	19.86	2.16	18.49	2.61	17.22	2.28	14.94	79.75	24	19.14	3.40	2.245	0.27	3.3
K032	1077	1124.85	17.98	2.16	18.49	2.59	20.16	2.65	17.51	97.43	28	27.28	3.83	2.08	0.21	5
K033	1099	1130.45	14.92	2.32	12.45	2.65	13.15	3.86	9.29	57.22	13	7.44	5.56	4.069	0.25	69.5
K033	1108	1133.30	16.52	2.31	12.83	2.63	14.43	4.28	10.15	64.14	14	8.98	3.76	9.82	0.14	60*
K034	1130	1137.82	15.25	2.29	13.58	2.61	16.00	3.78	12.22	73.07	19	13.88	4.91	4.487	0.15	
K034	1140	1140.74	21.19	2.26	14.72	2.59	19.28	7.19	12.09	92.27	19	17.53	5.29	5.17	0.19	20*
K034	1150	1143.15	16.43	2.28	14.15	2.61	13.56	1.90	11.66	60.03	21	12.61	2.80	2.081	0.1	
K035	1160	1145.93	13.55	2.42	8.68	2.70	9.15	5.40	3.75	37.36	9	3.36	3.73	7.221	0.16	40*
K035	1178	1150.45	8.56	2.36	10.94	2.61	16.52	8.76	7.76	75.78	22	16.67	4.53	9.017	0.22	122
K037	1210	1155.40	12.91	2.42	8.68	2.60	12.02	1.65	10.37	52.52	26	13.66	4.14	1.642	0.28	3.3
K037	1214a	1156.20	11.46	2.50	5.50	2.61	13.15	2.45	10.70	57.95	18	10.43	6.08	2.55	0.19	40
K037	1214b	1156.30	11.15	2.49	6.04	2.60	15.47	5.25	10.22	70.33	13	9.14	4.51	5.22	0.2	91
K037	1221a	1158.10	9.85	2.43	8.19	2.61	12.31	1.42	10.89	53.79	19	10.22	3.80	1.36	0.16	2
K037	1221b	1158.20	9.85	2.36	11.13	2.63	16.83	10.77	6.06	76.89	19	14.61	4.93	15.077	0.17	285*
K037	1222a	1158.30	9.85	2.35	11.49	2.62	14.59	7.38	7.21	65.13	13	8.47	4.86	9.14	0.17	231
K037	1222b	1158.40	9.85	2.46	7.36	2.61	14.32	6.72	7.60	63.95	12	7.67	4.23	6.97	0.16	290

Core #	Sample #	Depth m	sonic porosity %	gamma density g/cm3	gamma porosity %	Hg density g/cm3	Hg porosity %	macro porosity %	micro porosity %	Inj. Vol. mm3/g	We %	We mm3/g	PTD	Shg/Pc (max)	l sh	K mD
K038	1247	1165.64	0.42	2.37	10.75	2.63	14.55	1.46	13.09	64.68	19	12.29	2.90	1.152	0.17	0.25*
K038	1256	1168.55	5.31	2.44	7.92	2.61	9.72	0.97	8.75	41.20	26	10.71	1.84	1.146	0.15	0.001
K040	1299	1184.24	2.23	2.41	9.06	2.63	12.79	1.09	11.70	55.87	19	10.62	3.00	0.739	0.24	0.28
K042	1336	1196.51	1.31	2.44	8.08	2.63	11.86	1.30	10.56	51.15	18	9.21	3.34	0.915	0.14	0.09
K047	1366	1207.91	3.54	2.36	10.94	2.66	15.85	6.18	9.67	70.77	16	11.32	5.34	5.912	0.19	9.1
K047	1376	1212.05	5.19	2.39	9.81	2.62	9.96	1.69	8.27	42.23	13	5.49	3.65	1.432	0.16	2.4
K048	1389	1216.96	7.93	2.32	12.64	2.63	18.32	8.06	10.26	85.22	12	10.23	5.32	7.815	0.17	104
K049	1419	1224.31	7.18	2.31	12.83	2.62	18.77	4.32	14.45	88.15	14	12.34	5.70	4.127	0.27	10
K050	1432	1229.14	11.79	2.28	13.96	2.59	17.61	5.28	12.33	82.70	13	10.75	5.27	5.128	0.16	31.3
K051	1452	1236.98	8.29	2.31	12.83	2.61	13.16	1.97	11.19	58.01	14	8.12	3.52	1.604	0.2	11.1
K052	1477	1249.32	15.75	2.31	12.83	2.62	12.34	2.47	9.87	53.65	20	10.73	3.25	2.096	0.19	74
K052	1485	1252.55	13.63	2.37	10.57	2.60	16.21	2.76	13.45	74.39	16	11.90	3.48	2.377	0.22	10
K053	1501	1256.68	14.82	2.28	14.15	2.61	17.14	3.43	13.71	79.38	14	11.11	4.64	3.265	0.25	5.6
K053	1504	1257.51	16.20	2.31	12.83	2.60	18.55	2.97	15.58	87.51	18	15.75	3.11	2.06	0.25	0.7
K054	1527	1265.55	8.36	2.38	10.19	2.62	12.55	1.32	11.23	54.84	15	8.23	2.67	1.034	0.19	1.3
K056	1597	1289.22	5.93	2.35	11.32	2.62	12.16	1.34	10.82	52.90	16	8.46	2.58	1.156	0.16	0.25
K058	1630	1301.40	7.22	2.37	10.57	2.60	14.53	3.10	11.43	65.49	12	7.86	4.55	2.783	0.28	5
K059	1659	1311.08	12.66	2.31	12.83	2.64	13.56	1.21	12.35	59.49	17	10.11	2.14	0.824	0.19	0.15
K060	1690	1324.42	14.10	2.27	14.34	2.63	15.23	4.68	10.55	68.30	10	6.83	5.12	3.92	0.31	12.5
K061	1700	1327.04	12.80	2.30	13.21	2.63	14.37	2.14	12.23	63.91	16	10.23	3.56	1.976	0.19	3.1
K061	1705	1329.62	11.27	2.20	16.98	2.60	18.55	2.14	16.41	87.53	14	12.25	3.49	2.125	0.22	5.3
K061	1715	1332.46	11.56	2.24	15.47	2.62	15.90	5.07	10.83	72.28	16	11.56	5.34	4.491	0.23	8.4
K061	1726	1335.56	16.05	2.17	18.11	2.61	16.01	2.95	13.06	73.11	11	8.04	3.99	2.676	0.18	5
K062	1745	1339.92	14.54	2.33	12.08	2.63	15.27	1.88	13.39	68.50	24	16.44	3.22	1.459	0.36	0.55
K062	1760	1344.01	13.37	2.30	13.21	2.62	15.30	2.11	13.19	68.95	15	10.34	3.87	1.869	0.22	1.18
K065	1785	1350.98	10.70	2.39	9.96	2.65	8.96	0.77	8.19	37.21	20	7.44	3.07	0.725	0.31	0.001
K065	1802	1357.49	7.40	2.32	12.60	2.64	11.63	1.02	10.61	49.92	26	12.98	3.19	0.905	0.46	0.5
K066	1818	1363.07	12.63	2.35	11.32	2.63	14.21	0.51	13.70	62.91	23	14.47	3.31	0.86	0.39	0.037
K067	1836	1368.65	10.39	2.36	10.94	2.65	12.97	0.66	12.31	56.17	29	16.29	2.59	0.615	0.43	0.025
K068	1877	1381.44	7.25	2.39	9.81	2.65	2.64	0.41	2.23	10.24	23	2.36	2.73	0.451	0.42	0.001
K070	1912	1391.06	6.43	2.42	8.68	2.63	11.54	0.60	10.94	49.55	23	11.40	2.78	0.441	0.49	0.001
K070	1942	1398.65	12.50	2.37	10.57	2.65	9.51	0.76	8.75	39.66	35	13.88	2.30	0.595	0.68	0.001
K071	1951	1402.08	12.09	2.34	11.70	2.64	11.67	0.78	10.89	50.11	23	11.53	2.27	0.752	0.5	0.001

* perméabilité à l'eau

APPENDIX 3

A semi-quantitative analysis of the different minerals is proposed. This analysis is based on visual evaluation with the Chilingar chart. It gives the total amount of each phase in matrix and/or fractures.

Depth (m)	FRACTURE Fracture volume %	PRIMARY PHASES											DIAGENETIC PHASES										DISSOLUTION			POROSITY	
		Detritic quartz	Detritic feldspath	Heavy minerals	Mica	Mud clast	Volcanic lithoclast	Crystalline lithoclast	Clay minerals	Anhydrite	Carbonate	Opaque	Quartz overgrowth 1	Feldspath neogenesis	Kaolinite in feldspath	Quartz overgrowth 2	Ankerite	Siderite	Quartz overgrowth 3	Anhydrite	Barite	Opaque	Feldspath dissolution	Barite dissolution	Pressure-dissolution	Total porosity %	Maximum porosity %
952.10	20	0	0	0	0	0	0	15	9.5	42	6.5	0	0	0	0	5	0	0	18	0	4	0	0	0	0	0	
969.74		0	0	0	0	0	0	22	0	66	0	0	0	0	0	0	0	0	0	0	0	0	0	0	0	0	
1013.90		31	15	0.8	8	0	0	12	0	0	0.4	4.4	0	0	0	8	0	0	0	0	0	0.8	0	5	0	9	
1023.81		30	17	1	10	5	15	0	5	0	0	3	0	0	15	0	2	0	0	0	0	0	0	5	0	3	
1035.66		25	10	1	3	5	5	10	0	0	0	5	0	0	5	0.1	0	0	0	0	0	0	5	15	5		
1041.58	5	28.5	9.5	0	0.95	0	9.5	9.5	4.75	0	4.75	1.9	1.9	0	10	2.85	4.25	0	0	0	0.25	0	3.8	0	0		
1049.54		30	15	0	5	0	10	5	10	0	0	2	0	0	0	5	0	0	0	0	0	0	2	15	5		
1057.92		38	5	0.8	3	2	8	7	15	0	0	1	1	1.2	0	5	0	0	0	0	0	1.6	0	2	11.6	7.2	
1073.05		34	9	0	0	0	0	13.5	11	0	0	9	0.7	0.7	0.9	0	0	0	0	0	0	0.9	0	0.7	9	0	
1076.76		30	10	0.5	0	0	5	5	12.5	0	0	3	0.5	2.5	0	0	0	0	0	0	5	2.5	0	4	10	2.5	
1081.10		30	10	0	0	0	0	10	15	0	0	2	0	2	0	0	0	0	0	5	5	5	0	2	15	0	
1082.04		40	15	0	0	0	0	10	10	0	0	1	1	0	0	0	0	0	0	0	0	1	0	2	10	2	
1083.39		35	10	0	0	0	3.5	10	0	0	0	0.6	0.3	0.6	0	0.7	0	0	0	0	4.5	0	0	0.9	17	0.6	
1083.72		38	5	0	0	0	7	16	16	0	1.8	0	0	0.6	0	0	0	0	0	0	0	0.6	0	0.4	14	0	
1085.52		40	5	0	0	0	5	5	10	0	0	3	2	1	5	0	0	0	0	0	0	0	0	5	0	0	
1087.30		35	10	0.6	0	0	5	5	5	0	0	1.2	0	0.6	3	4	0	0	0	0	6	0.6	0	3	10	0	
1088.93	30	24.5	5.25	0	0	0	3.5	7	5.25	0	2.45	0.35	0	0	8.5	0	0	21	0	0	4.5	0.7	0	0.35	10	0.7	
1094.31		32.5	12.5	0	1	0	5	7.5	12.5	0	0	1	0.5	2	0	0	0	0	0	0	1.5	0.5	0	2.5	12.5	2.5	
1097.82	10	27	9	0	0	0	9	9	0.9	0	0	0.9	0	0	14	0	0	4	1.8	0	5.8	0	0	0.9	10.5	1.8	
1104.92		38	11	0	0	0	6	5	6	0	0.4	2	0.2	1	8	0	0	0	0	0	0	0.8	0	2.6	4.6	1.6	
1106.68	35	22.75	9.75	0	0	0	3.25	6.5	6.5	0	3.25	1.3	0	0	0	0	0	1.75	0	33.25	0	1.3	0	1.95	3.25	0.65	
1114.96		27.5	12.5	0	0.5	0	12.5	12.5	5	0	1	2.5	0	0.5	0	0	0	2.5	0	2.5	0	1.5	5	6.5	15	1	
1119.29		30	11.5	0	0.4	0	5.5	11.5	2.2	0	0	1	0	0	9	0	0	3.5	0	0	0	3.4	3.9	1.8	15.2	0	
1123.74		20	10	0.7	0	0	13.5	11.5	9.1	0	0	2	0	0.3	0	0	0	0	0	0	0	2.4	0	5	9.4	4.1	
1125.90		25	10	0	0	0	10	10	10	0	0	5	2	1	1	2	0	1	0	0	0	3	0	5	14	4	
1130.54		20	10	1	0	0	10	15	3	0	0	2	0	0	6	0	0	3.5	0	5	0	5	5	2	15	0	
1133.07		0	0	0	0	0	0	0	0	0	0	0	0	0	0	0	0	0	0	0	0	0	0	0	0	0	
1137.86		18	10	0	0	0	18	12	8.2	0	1.2	0.6	0	1.6	0	0	0	0	0	0.8	0	3	4	1.8	15	0	
1143.20		13	6.5	0	0	0	10	17	11.5	0	1.5	1.4	0	1.3	0	0	0	0.6	0	1.5	0	2.3	3.5	1.4	54.6	1.6	
1145.98		0	0	0	0	0	0	0	0	0	0	0	0	0	0	0	0	0	0	0	0	0	0	0	0	0	
1155.44		0	0	0	0	0	0	0	0	0	0	0	0	0	0	0	0	0	0	0	0	0	0	0	0	0	
1156.36		32.5	8.5	0	0	0	12.5	12.5	3.75	0	0	0.5	0.5	0	3.75	0.5	0	1.25	0	2.5	0	0.5	0	1	10	3.75	
1168.60		25	10	0	2	0	12.5	12.5	7.5	0	0	0	0	1	5	0	0	0	0	0	1	1	0	0	5	1	
1171.96	20	32	8	0.8	0	0	4	4	4	0	0	1.6	0	0	7	3	0	4	0	10	0	0	1.6	1	0		
1184.31		29	9.5	1.4	0	0	10	9.5	0	0	0.5	0	0	1.9	9	1	0	0	0	0	5.5	4.7	0	0	10.75	0	
1189.40	10	31.5	9	0	0	0	9	9	2.7	0	0	0.9	0.9	0	9.5	0	0	0.5	0	9	1.8	0	1.8	0.9	0	0	
1196.90		25	10	1	0	0	10	5	10	0	2	0	0	0	0	5	0	0	0	0	0	5	0	0	10	1	

Depth (m)	FRACTURE Fracture volume %	PRIMARY PHASES											DIAGENETIC PHASES											DISSOLUTION			POROSITY	
		Detritic quartz	Detritic feldspath	Heavy minerals	Mica	Mud clast	Volcanic lithoclast	Crystalline lithoclast	Clay minerals	Anhydrite	Carbonate	Opaque	Quartz overgrowth 1	Feldspath neogenesis	Kaolinite in feldspath	Quartz overgrowth 2		Ankerite	Siderite	Quartz overgrowth 3	Anhydrite	Barite	Opaque	Feldspath dissolution	Barite dissolution	Pressure-dissolution	Total porosity %	Maximum porosity %
1203.90	75	26.25	6	0.15	0	0	1	1	1.5	0	0	0	0	0	0	46.5	0	0	0	0	0	0	0	0.3	0	0	2.05	0
1204.00	50	17.5	7.5	0.5	0	0	2.5	2.5	5	0	0	2.5	1	0.5	0	7.5	7.5	0	0	7.5	0	30	2.5	0	0	2	4	0
1204.20	50	15	5	0	0.5	0	5	2.5	0	0	0	0	0	0	0	20	0	0	15	0	30	2.5	0	0	0	5	0	
1208.24		20	0	0	1	0	15	10	10	0	0	2	2	0	0	0	0	0	1	0	2	0	5	3	5	20	0	
1214.38	25	26.25	7.5	0	0	0	7.5	7.5	1.5	0	0	0	0.75	0	0	0	11.25	0	0	4	0	14.75	0.75	0	0	0.75	12.5	0
1217.32		20	10	0	0	0	15	15	5	0	0	0	2	0	0	3	0	0	0	1	0	3	0	5	3	5	25	0
1224.88		20	10	0	2	10	5	15	10	0	0	0	2	0	0	5	0	0	0	0	0	5	2	0	5	25	0	
1229.18		25	10	0	2	5	10	10	5	0	0	0	3	0	0	5	0	0	0	0	0	0	0	3	0	5	25	0
1237.64		30	10	0	0	0	10	15	5	0	0	0	2	0	1	5	0	0	0	0	0	0	0	2	0	3	10	2
1249.37		30	0	0	0	0	10	10	5	0	0	0	3	0	0	3	0	0	0	0	0	0	0	3	0	3	25	0
1252.66		25	10	0	0	0	5	15	15	0	0	2.5	0	0	0	1	0	0	0	0	0	0	5	0	2	22.5	0	
1256.70		20	10	1	0	0	5	10	5	0	0	5	2	0	2	0	0	4	0	0	0	0	0	3	0	3	20	0
1257.72		25	10	0	0	0	5	10	8	0	0	0.4	0	0	0	0	0	5	0	0	0	0	0	2	0	0	17	0
1263.95		30	10	0	0	0	10	10	5	0	0	1	3	2	0	10	0	0	0	0	0	0	5	0	5	20	0	
1289.79		30	10	0	0	1	10	10	5	0	0	2	2	0	0	10	0	1	0	1	0	1	0	5	0	2	17.5	0
1293.74	25	27.25	8	0	0	0	8	0.5	1.5	0	0	0	0.75	0	0	7.5	0	1.5	0	2.5	0	16.5	3.75	2.25	0	0.75	12.5	1.5
1301.67		25	10	0	0	0.95	14.75	14.75	9.5	0	0	0	4.75	0	0	0	0	1.25	0	0	0	0	0	0	0	4.75	19.5	0
1311.64		25	15	1	1	0	10	5	5	0	0	0	5	0	0	5	0	1	0	0	0	1	3	5	0	5	15	0
1324.47		30	10	0	0	0	10	10	5	0	0	0	5	0	0	5	0	1	0	0	0	0	0	3	0	5	10	0
1327.66		21.25	9.75	0	0	0	10	10	4.75	0	0	5.25	2	0	0	10.5	0	4.75	0	0	0	0	2.85	0	2	11.88	0	
1329.77		35	10	0	0	1	10	10	5	0	0	0	3	0	0	2	0	3	0	0	0	0	5	2	0	3	20	0
1335.61		35	7	0	0	0	10	10	10	0	0	0	2	0	0	2	0	3	0	1	0	1	0	3	0	2	10	2
1339.97		34.5	10	0.8	0	0	4.5	5	6.7	0	0	3.4	1.8	0	0	0	0	2	0	0	0	2.4	0	0	1.8	19.5	0	
1348.14	25	27.5	10.5	0	0.7	2	5	5	5.5	0	0	0	0	2	-1.1	4	7.5	0	0	2.5	0	6.25	0.7	0	0	0	7.3	0
1351.02		30	5	1	0	5	5	5	10	0	0	5	5	0	3	7	0	7	0	0	0	1	0	5	0	5	10	2
1358.30		35	5	1	0	5	5	5	15	0	0	3	2	0	0	0	0	1	0	0	0	1	0	1	0	2	15	3
1359.01		7	1.4	0	0	0	1	1	6	0	24	31	0	0	0	0	0	24	0	0	0	0	0	0	0	0	0	0
1363.41		25	10	1	0	5	10	10	17.5	0	0	3	1	0	0	0	0	0	0	0	0	2	3	0	1	10	1	
1365.29		15	4	2.5	0	0	2.5	2.5	0	0	10	22.5	0	0	0	0	0	10	0	0	0	0	0	0	0	0	0	0
1368.80		30	10	0	1	10	10	10	10	0	0	5	1	1	0	2	0	2	0	0	0	0	0	1	0	1	3	0
1376.96	20	24	8	0	0	4	8	8	4	0	4	0	4	4	0	2	2	8	0	0.8	0	8.4	0	0	0	4	10	0
1381.49		35	10	3	1	1	5	5	15	0	0	2	1	0	0	1	0	0	0	0	0	0	0	0	1	0	0	0
1391.12		24	14.2	0	0	4.5	0	9.5	13.5	0	0	4.5	0.9	0.9	0	0	0	13	0	0	0	0	0.9	0	1.8	4.6	2.7	
1399.15		26.75	0	0	0	0.9	5	10	13.5	0	0	2.7	0.9	0	0.9	0	0	2	0	0	1.6	0	0	0.9	0	0.9	4.5	0
1402.15		29.75	9.75	1.9	0	5	5	5	14.25	0	0	4.75	1.9	0.95	0	2.85	0	1.75	0	0	0	0	0	0	2.85	2.85	1.95	
1411.50		25	15	0	0	5	10	10	15	0	0	0	2	0	0	3	0	3	0	0	0	0	2	0	2	5	2	
1416.26	10	27	9	0	0	0	9	9	4.5	0	0	4.5	2.7	1.8	0	0	0	13.5	0	2	0	8	0	0	4.5	0	0	
1416.33		35	10	0	0	0	5	0	5	0	10	0	2	1	0	10	0	15	0	5	0	0	0	0	3	0	0	0

